Available online at www.sciencedirect.com
SCIENCE DIRECT®
Physica D 198 (2004) 281–308
PHYSICA D
www.elsevier.com/locate/physd

Diffuse interface modeling of two-phase flows based on averaging: mass and momentum equations

Y. Sun, C. Beckermann*

Department of Mechanical and Industrial Engineering, The University of Iowa, Iowa City, IA 52242, USA

Received 23 April 2004; received in revised form 26 August 2004; accepted 7 September 2004

Communicated by M. Vergassola

Abstract

A diffuse interface model is derived for the direct simulation of two-phase flows with surface tension, phase-change, and density and viscosity differences between the phases. The derivation starts from the balance equations for a sharp interface and uses an ensemble averaging procedure on an atomic scale to obtain a diffuse interface version of the equations. As opposed to thermodynamically derived models, the two phases are assumed to coexist inside the diffuse interface with different properties, velocities, and pressures. Separate conservation equations are solved for each phase. The phase interactions are modeled explicitly through the inclusion of interfacial forces in the momentum equations for each phase. Based on a superposition of microscopic (atomic-scale) and macroscopic interface morphologies, an expression for the interfacial momentum source due to surface tension is introduced that is equivalent to the capillary stress term encountered in thermodynamically derived models. Also, a constitutive relation for the average viscous stresses of each phase inside the diffuse interface is presented. The model is tested for simple one-dimensional flows tangential and normal to a diffuse interface, and the results are compared to those obtained from a thermodynamically derived model.
© 2004 Elsevier B.V. All rights reserved.

PACS: 47.55.Kf; 05.70.Fh; 68.10.Cr

Keywords: Diffuse interface model; Two-phase flow; Surface tension; Averaging

1. Introduction

Diffuse interface methods have been a popular tool in the direct simulation of two-phase flows [1]. In such methods, the interface between the two phases has a finite width and is characterized by rapid but smooth transitions

* Corresponding author. Tel.: +1 319 335 5681; fax: +1 319 335 5669.
E-mail address: becker@engineering.uiowa.edu (C. Beckermann).

0167-2789/$ – see front matter © 2004 Elsevier B.V. All rights reserved.
doi:10.1016/j.physd.2004.09.003

in the density, viscosity, and other physical quantities. An order parameter or phase indicator function ϕ is introduced to represent the transition between the phases. A unique set of conservation equations (i.e., mass and momentum) is solved over the entire domain by letting the properties vary across the interface. The evolution of ϕ in the domain is computed from a separate equation. Distributed interfacial sources are introduced into the conservation equations to account for surface tension [2], interfacial drag [3], or other effects. The volume-of-fluid (VOF) [4], level-set [5], lattice-Boltzmann-equation (LBE) [6–9], and phase-field methods [10] are sometimes or always associated with diffuse interface approaches [1]. The major advantage of diffuse interface methods is that explicitly satisfying sharp interface conditions is avoided and changes in the interface topology are easily handled. However, in many physical situations the actual interface width is only of the order of nanometers. Hence, problems can arise if the interface is artificially smeared in order to reduce computational requirements. However, asymptotic analyses have been devised to allow computations to be performed for larger interface widths without a loss in accuracy [3,10].

The governing equations for diffuse interface methods can be derived from thermodynamically consistent theories of continuum phase transitions [1,10–14] or from gradient theories [15,16]. For example, Jacqmin [11] used thermodynamic principles to obtain a diffuse interface model for two-phase flows and clarified the form of the continuum surface tension force term. Most recently, Anderson et al. [12] performed a thermodynamic analysis to derive a very general diffuse interface model for two-phase flows in the context of the phase-field method and identified a number of new non-equilibrium terms inside the diffuse interface. The corresponding sharp interface equations can be obtained from diffuse interface models by performing an asymptotic analysis for a vanishing interface width [17].

Beckermann et al. [3], in a study of solidification related phenomena, applied for the first time a formal ensemble (or volume) averaging procedure [18,19] to derive the equations for a diffuse interface directly from the local, sharp interface equations. In the past, averaging has only been used to derive models for large-scale systems where the radius of curvature of the interface is small compared to the size of the system. Examples can be found in the analysis of bubbly or particulate flows in engineering equipment, porous media, soil mechanics, glaciology, oil recovery, magma dynamics, metal solidification, earthquake dynamics, mantle flow, and many others (see Refs. [18–24] and references therein). Ensemble averaging can be viewed as a simple version of more general homogenization techniques that have been applied to a variety of multi-phase systems [25,26]. In these large-scale models, the actual shape and motion of the interface is not resolved and the interactions between the phases are only accounted for in an average sense.

When using averaging to derive a model for a diffuse interface, as in Beckermann et al. [3], averaging is applied on a much smaller, atomic scale in order to resolve the flows inside the diffuse interface and the motion of the interface. Such an averaging approach is adopted here to derive the mass and momentum equations for a rather general two-phase system that consists of two Newtonian fluids or a fluid and a rigid solid (but the solid is not modeled). Surface tension, phase-change, and density and viscosity differences between the phases are all considered. Since in the averaging approach the equations for a diffuse interface are derived "backward" (relative to the thermodynamic treatments) from well-established local, sharp interface equations, the connection between diffuse and sharp interface models is much clearer than in thermodynamic approaches [17] and several new insights can be obtained.

While many of the present concepts are adopted directly from traditional two-phase flow theories [18–22], a superposition of macroscopic and atomic-scale interface morphologies is introduced that is only applicable to diffuse interface modeling. This superposition assumes that the radius of curvature of the interface is large compared to the diffuse interface width. With that assumption, an expression for the capillary stress tensor for a diffuse interface is derived that is equivalent to the one obtained from thermodynamic theories [1,11]. The superposition also results in the derivation of a previously unidentified interfacial force that is associated with curvature variations in the presence of surface tension. Several other modeling elements introduced in this study would also be useful in large-scale two-phase models that do not involve a diffuse interface [18,19], including rather general models for the averaged shear stresses and interfacial drag forces of the phases in a two-fluid system.

To the best of our knowledge, all thermodynamically derived models for two-phase flow assume the existence of a single velocity and pressure at any point inside the diffuse interface. These variables can vary steeply across the interface, depending on the two-phase flow situation. Moreover, a single density and viscosity are assumed to exist and their variation across the diffuse interface needs to be postulated in some ad-hoc manner, because thermodynamics does not usually provide the variation (unless the properties themselves are used as the order parameter). For large differences in these properties between the phases, this can lead to results that are very dependent on the way the property variations are specified. The present averaging approach offers an alternative by treating each phase separately and assuming the coexistence of the two phases inside the diffuse interface. In such a two-phase approach, which is rather common for modeling large-scale systems [18–23], each phase possesses its own velocity, pressure, and physical properties. Separate (averaged) conservation equations are solved for each phase. The phase interactions are modeled explicitly through the inclusion of distributed interfacial terms in the averaged equations. In the present study, such a two-phase approach is adopted for modeling the flow inside a diffuse interface. This avoids the potentially steep variations of the variables across the diffuse interface, and the property variations follow naturally from the derivations. The two-phase approach implies that a slip flow can exist between the phases inside the diffuse interface, which is proposed here as a more realistic model for cases with large density and viscosity differences between the phases. A complication inherent in this approach is that not much is known about the interactions between the phases inside a diffuse interface containing atomic-scale structures. Thus, an important objective of the present study is to derive phase interaction terms for a diffuse interface.

By simply adding the averaged mass and momentum conservation equations for each phase, and making use of averaged interfacial balances, a so-called mixture model can be derived from the present two-phase model. Assuming furthermore equal velocities of the two phases inside the diffuse interface, a direct connection with thermodynamically derived models [11,12] can be made. Comparisons between the two modeling approaches are performed throughout the paper.

Finally, it is important to mention the issue of interface width. In simulating two-phase systems that are large compared to the actual interface width, the width must usually be chosen artificially large to allow for proper numerical resolution. There are some instances, however, where the interface width is of the same order as the length scale of the phenomena being investigated and the width must be chosen realistically. Examples include near-critical fluids, contact line motion, breakup or merging of interfaces, spinodal decomposition, solute trapping in rapid solidification, etc. [1,10]. In the present study, special attention is paid to this issue by examining how the model results behave with changing interface width. For this purpose, the model equations are solved for several simple flows. It is shown that the two-phase model results are generally independent of the interface width, except in those cases that involve surface tension. This is a critical property in simulations of larger scale two-phase flows.

This paper focuses solely on the derivation of the mass and momentum conservation equations for a diffuse interface. The derivation of an equation for the propagation of the interface in non-equilibrium situations (i.e., the phase-field equation), using the same two-phase averaging approach, will be presented in a forthcoming publication. In order to keep the derivations reasonably simple, the flow inside the diffuse interface is assumed to be slow enough that the momentum dispersion term that arises in the averaging process can be neglected. This appears reasonable, in part because such a term does not arise in thermodynamic models. The interfacial Reynolds number, based on the interface width and the relative velocity between the two phases, is assumed to be small enough that the drag force inside the diffuse interface can be modeled as being linearly proportional to the slip velocity. Furthermore, all thermophysical properties of the two phases are assumed uniform inside an averaging volume (but they may vary globally). Again, more complex models do not appear to be justified in the present context.

In Section 2, the averaging procedures and the two-phase approach are explained in more detail. The superposition of interface morphologies and a model for the average curvature of a diffuse interface are presented in Section 3. The derivation of the averaged mass and momentum conservation equations, starting from the local equations for a sharp interface, is described in Section 4. The modeling of the average stresses, the interfacial momentum source term, and the interfacial force density is discussed in Sections 5–7, respectively. In Section 8, the model results are examined for simple one-dimensional two-phase flow systems. A brief summary is provided in Section 9.

2. Averaging and two-phase approach

In the present study, averaging is applied on the scale of the fluctuating atomic structures inside the diffuse interface to obtain a model that allows for the direct simulation of the motion and shape of interfaces in two-phase flows. Averaging serves to derive the governing equations for the diffuse interface where the two phases are assumed to coexist and the dependent variables are necessarily a function of the phase function ϕ. An averaging volume ΔV can be chosen that is small compared to the width of the diffuse interface, l_i, but large compared to the characteristic length of the atomic structures inside the interface, l_a. In many applications this would imply that the averaging volume has a "radius" of the order of nanometers. For a diffuse interface model to be valid there is the additional constraint that l_i must be much smaller than the characteristic radius of curvature of an interface, l_c. More rigorously, the phase function ϕ is defined as the ensemble average of an existence function, X_1, which is unity in phase 1 and zero otherwise, via $\phi = \phi_1 = 1 - \phi_2 = \langle X_1 \rangle$. The subscripts 1 and 2 denote any phase k in a two-phase system. The parentheses $\langle \cdot \rangle$ denote an ensemble average, such that an averaging volume ΔV actually does not need to be specified [18]. For ease of visualization, however, the notion of a volume average will be used in subsequent portions of the paper. The phase function ϕ can then be interpreted as an atomic-scale volume fraction.

The present concept of defining ϕ as the ensemble average of an existence function on an atomic scale is perhaps not too different from the phase-field method where ϕ is viewed as an order parameter [10]. Such an order parameter describes the probability of an atom to occupy a particular location, for example in a crystal lattice.

Averaging has been established as a rigorous mathematical procedure [18,19]. Here, only some important averaging rules are reviewed. The ensemble averaging process satisfies the following Reynolds', Leibniz', and Gauss' rules, respectively [18]

$$\langle f + g \rangle = \langle f \rangle + \langle g \rangle, \quad \langle \langle f \rangle g \rangle = \langle f \rangle \langle g \rangle, \quad \text{and} \quad \langle c \rangle = c \tag{1}$$

$$\left\langle \frac{\partial f}{\partial t} \right\rangle = \frac{\partial}{\partial t} \langle f \rangle \tag{2}$$

$$\left\langle \frac{\partial f}{\partial x_i} \right\rangle = \frac{\partial}{\partial x_i} \langle f \rangle \tag{3}$$

where f and g are sufficiently well behaved functions so that the limiting processes of integration and differentiation can be interchanged [18], c a constant, t time, and x_i is a spatial coordinate. Gauss' rule, Eq. (3), is valid because the present filter function is homogeneous (i.e., it is unity) [27]. For the existence function, X_k, Eqs. (2) and (3) lead to $\partial \phi_k / \partial t = \langle \partial X_k / \partial t \rangle$ and $\nabla \phi_k = \langle \nabla X_k \rangle$, respectively. The latter equation should not be confused with the average of the derivative of the existence function in the direction normal to the interface, i.e., $\langle |\nabla X_k| \rangle = \langle -\partial X_1 / \partial n \rangle$. Since $|\nabla X_k|$ behaves as a Dirac delta function, picking out the interface, its average is nothing but the interfacial area per unit volume S [18], i.e.

$$S = \langle |\nabla X_k| \rangle \tag{4}$$

Another important relation associated with the existence function is that X_k is advected by the local interfacial velocity, $\boldsymbol{u}_\mathrm{i}$, between the phases according to [18]

$$\frac{\partial X_k}{\partial t} + \boldsymbol{u}_\mathrm{i} \cdot \nabla X_k = 0 \tag{5}$$

The above relations are used in the following sections to derive the averaged equations for a diffuse interface directly from the local, sharp interface equations.

The two-phase approach is illustrated in detail in Fig. 1. There are several cases that are distinguished in the present study:

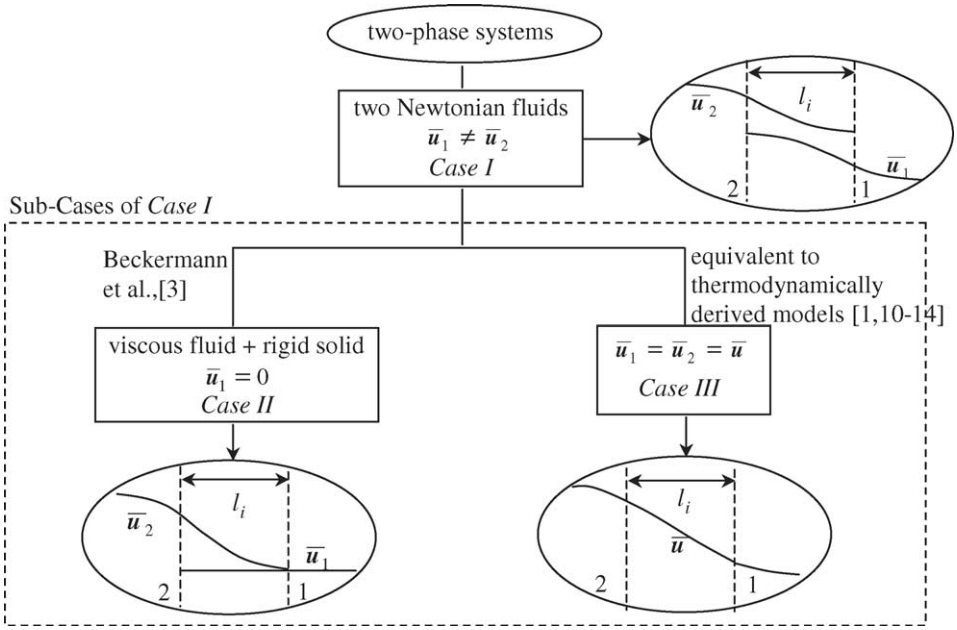

Fig. 1. Schematic illustration of the present two-phase approach.

- *Case I*: The system consists of two Newtonian fluids of arbitrary viscosity and density. The velocities (and pressures) of the two phases inside the diffuse interface are different, i.e., a slip flow is allowed. This is the most general case and the main focus of the present study. Following Ref. [12], a solid–fluid system may be modeled by assigning a large viscosity to the solid.

As illustrated in Fig. 1, Cases II and III should be viewed as sub-cases of Case I, because the governing equations for Cases II and III follow directly from the ones for Case I.

- *Case II*: If the solid phase (say phase 1) in a solid–fluid system can be assumed to be rigid and stationary, it is appropriate to simply assign a velocity of zero to the solid and not solve any equations for the solid phase (instead of assigning a large viscosity to the solid and still solving the equations for the solid phase). Then, the solid phase does not need to be viewed as a Newtonian fluid. This approach is the same as in Beckermann et al. [3]. The diffuse interface in Case II can be viewed as a porous medium and classical theory for porous medium type flows can be used to justify some of the modeling.
- *Case III*: The velocities of the two phases inside the diffuse interface are assumed equal. This case is referred to as a *mixture* model and is intended to mimic thermodynamically derived models for diffuse interfaces between two fluids. It is mainly included here in order to allow for a detailed comparison with thermodynamically derived models. However, the assumption of equal velocities may actually be quite appropriate for cases where the densities and viscosities of the two phases are not too different.

3. Superposition of interface morphologies

Critical to the present method is the modeling of the interface morphology, and this is where the present approach significantly differs from traditional averaging of large-scale two-phase systems. Fig. 2 illustrates the three-length scales l_c, l_i, and l_a in decreasing order from left to right. The *local* unit vector normal to the atomic-scale structures

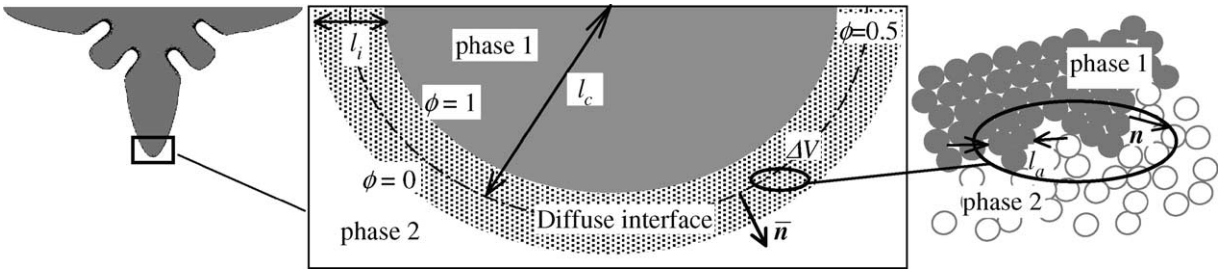

Fig. 2. Schematic illustration of interface morphologies at different scales.

inside the diffuse interface, $\boldsymbol{n}$, and the corresponding *local* curvature, κ, are given, respectively, by (see Ref. [18] on how to differentiate the binary existence function X_k using a set of "test functions")

$$\boldsymbol{n} = -\frac{\nabla X_1}{|\nabla X_1|} \quad \text{and} \quad \kappa = \nabla \cdot \boldsymbol{n} = -\frac{1}{|\nabla X_1|}\left[\nabla^2 X_1 - \frac{(\nabla X_1 \cdot \nabla)|\nabla X_1|}{|\nabla X_1|}\right] = -\frac{1}{|\nabla X_1|}\left[\nabla^2 X_1 - \frac{\partial^2 X_1}{\partial n^2}\right] \tag{6}$$

where $|\nabla X_1| = -\partial X_1/\partial n$ and κ is positive when the interface is convex toward phase 2. An *average* unit normal vector, $\bar{\boldsymbol{n}}$, and an *average* curvature, $\bar{\kappa}$, can be defined, respectively, as (see Fig. 2)

$$\bar{\boldsymbol{n}} \equiv \frac{\langle \boldsymbol{n}|\nabla X_1|\rangle}{\langle|\nabla X_1|\rangle} \quad \text{and} \quad \bar{\kappa} \equiv \frac{\langle \kappa|\nabla X_1|\rangle}{\langle|\nabla X_1|\rangle} \tag{7}$$

where the denominator is nothing but S. Substitution of Eq. (6) into Eq. (7) to obtain $\bar{\boldsymbol{n}}$ and $\bar{\kappa}$ would require the exact knowledge of the local atomic-scale interface morphology.

To make progress, a simple model for the interfacial area per unit volume, S, is proposed here. It is assumed that S can be expressed as an algebraic function of ϕ and is not a function of the interface curvature on a macroscopic scale. This concept is illustrated in Fig. 3, where the interface is depicted as a superposition of macroscopic and microscopic (atomic-scale) morphologies. Recall from Eq. (4) that S is governed by the entire structure of the diffuse interface, and includes contributions from both the average curvature of the interface and the atomic-scale structure inside the diffuse interface (which exist even for a macroscopically flat interface). However, since $l_c \gg l_i$, S is assumed to be dominated by the fluctuating, atomic-scale structure inside the diffuse interface. With that assumption, S varies only across the diffuse interface (in the $\bar{\boldsymbol{n}}$ direction), but not along contours of constant ϕ. A model of this variation, assuming an isotropic diffuse interface morphology, is proposed here as

$$S = S_0 \phi^a (1-\phi)^b \tag{8}$$

where S_0, a, and b are constants that depend on the atomic-scale structure of a (flat) diffuse interface. The pre-factor S_0 is proportional to $1/l_i$ (see discussion following Eq. (9)). According to Eq. (8), the interfacial area per unit volume,

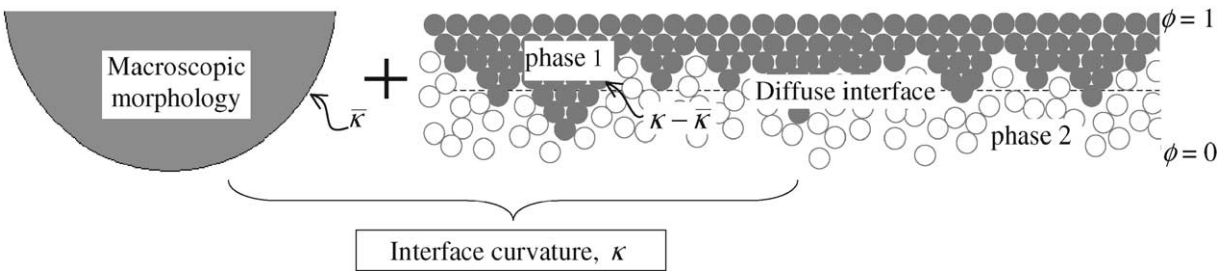

Fig. 3. Superposition of macroscopic and microscopic interface morphologies.

S, vanishes in the bulk phases and reaches a maximum at $\phi = \phi_c = a/(a+b)$. As shown below, it is usually necessary for S to be phase-invariant, which can be accomplished by choosing $a = b$. While it is difficult to relate the constants a and b explicitly to the atomic structure of an interface, an interesting connection can be made with the thermodynamic treatment used in phase-field methods [10]. It can be shown [28] that the interfacial area per unit volume, S, is related to the free energy density function, f, that is used in phase-field methods by $\mathrm{d}f/\mathrm{d}\phi = S\,\mathrm{d}S/\mathrm{d}\phi$. Choosing a symmetric double-well potential for f [10,12,13], which is proportional to $\phi^2(1-\phi)^2$, corresponds to $a = b = 1$ in Eq. (8). A bilinear potential [29], $\phi(1-\phi)$, coincides with $a = b = 1/2$. Additional discussion on the merits of different choices for a and b can be found in subsequent sections. Other functional forms for S are certainly possible, and Eq. (8) should only be viewed as an attempt to provide a specific example that appears to be physically meaningful.

The assumption that S varies only across the diffuse interface and is independent of the macroscopic interface curvature motivates the following relation between the interfacial area per unit volume and the gradient of ϕ in the $\bar{\boldsymbol{n}}$ direction

$$S = \langle |\nabla X_1| \rangle = \left\langle -\frac{\partial X_1}{\partial n} \right\rangle = -\frac{\partial \phi}{\partial \bar{n}} = |\nabla \phi|. \tag{9}$$

It is emphasized here that Eq. (9), i.e., $\langle \partial X_1/\partial n \rangle = \partial\phi/\partial\bar{n}$, is not a mathematically exact statement, because it is not compatible with the definition of $\bar{\boldsymbol{n}}$ given by Eq. (7). Instead, Eq. (9) should be viewed as an approximate model for the gradient of ϕ in the direction normal to the interface. This model is consistent with the assumption inherent in Eq. (8) that ϕ varies only across the diffuse interface and is independent of the macroscopic interface curvature. Eq. (9) represents the primary departure of the present model from traditional averaging of large-scale two-phase systems; in large-scale systems, where the volume fraction ϕ can vary in an arbitrary fashion on a macroscopic scale, the normal gradient of ϕ can generally not be related to the local interfacial area per unit volume, S. Note that Eq. (9) also implies that $\langle \partial^2 X_1/\partial n^2 \rangle = \partial^2\phi/\partial\bar{n}^2$.

By specifying the values for a and b in Eq. (8), Eq. (9) can be solved to obtain an "equilibrium" ϕ profile across the diffuse interface. For example, taking $a = b = 1$, it follows that $\partial\phi/\partial\bar{n} = -S_0\phi(1-\phi)$, which yields the hyperbolic tangent profile $\phi = [1 - \tanh(\bar{n}/2\delta)]/2$, where $\delta = 1/S_0$. Since ϕ varies from 0.05 to 0.95 over a distance of approximately 6δ, it is clear that $1/S_0$ is indeed a measure of the interface width l_i. For $a = b = 1/2$ and $S_0 = 1/(2\delta)$, a sinusoidal profile, $\phi = [1 - \sin(\bar{n}/2\delta)]/2$, is obtained with $l_i \approx 5\delta$. The above hyperbolic tangent and sinusoidal profiles for ϕ hold regardless of the average curvature of the interface. They are commonly encountered in the phase-field method [10,12,29]. The thermodynamic treatment used in the phase-field method also motivates a more exact definition of the interface width, l_i. In the phase-field method, the interface width is inversely proportional to the integral of the gradient energy per unit area of the interface, such that $1/l_i = \int_{-\infty}^{\infty} (\partial\phi/\partial\bar{n})^2\,\mathrm{d}\bar{n}$ [10]. Substitution of Eq. (9) yields the following relationship between l_i and S in the present model: $1/l_i = \int_{-\infty}^{\infty} S^2\,\mathrm{d}\bar{n}$. Then, it is easy to show that $l_i = 6/S_0 = 6\delta$ for $a = b = 1$ (i.e., the hyperbolic tangent profile) and $l_i = 8/(\pi S_0) = 16/\pi\delta \approx 5\delta$ for $a = b = 1/2$ (i.e., the sinusoidal profile).

Substituting Eq. (6) into Eq. (7), and using Eq. (9) as well as the identities $\langle \nabla X_1 \rangle = \nabla\phi$ and $\langle \nabla^2 X_1 \rangle = \nabla^2\phi$, it is easy to show that the average unit normal vector and average curvature are now given, respectively, by

$$\bar{\boldsymbol{n}} = -\frac{\nabla\phi}{|\nabla\phi|} \quad \text{and} \quad \bar{\kappa} = \nabla\cdot\bar{\boldsymbol{n}} = -\frac{1}{|\nabla\phi|}\left[\nabla^2\phi - \frac{(\nabla\phi\cdot\nabla)|\nabla\phi|}{|\nabla\phi|}\right] = -\frac{1}{|\nabla\phi|}\left[\nabla^2\phi - \frac{\partial^2\phi}{\partial\bar{n}^2}\right]. \tag{10}$$

While Eq. (10) may seem self-evident from a purely macroscopic point of view, it is again emphasized that they cannot be directly derived by averaging the microscopic (atomic-scale) normal vector and curvature, unless the approximation given by Eq. (9) is assumed valid. The above expression for the average curvature can be further rewritten by noting from Eq. (9) that $\partial^2\phi/\partial\bar{n}^2 = -\partial S/\partial\bar{n} = -(\mathrm{d}S/\mathrm{d}\phi)(\partial\phi/\partial\bar{n}) = S\,\mathrm{d}S/\mathrm{d}\phi$. Thus

$$\bar{\kappa} = -\frac{1}{S}\left[\nabla^2\phi - \frac{\mathrm{d}S}{\mathrm{d}\phi}S\right] = -\frac{\nabla^2\phi}{S} + \frac{\mathrm{d}S}{\mathrm{d}\phi}. \tag{11}$$

The last term in Eq. (11), $\mathrm{d}S/\mathrm{d}\phi$, has the interesting property of being a microscopic curvature of the fluctuating atomic structures inside ΔV. This can be understood by considering the following simple example (after Ref. [20]). If the averaging volume ΔV contains N spheres of phase 1 and radius r, it follows that $\phi = N4\pi r^3/3\Delta V$ and $S = N4\pi r^2/\Delta V$. Thus, $\mathrm{d}S/\mathrm{d}\phi = (\mathrm{d}S/\mathrm{d}r)/(\mathrm{d}\phi/\mathrm{d}r) = 2/r$, which is nothing but the curvature of a sphere of radius r. Using Eq. (8), a general expression for the microscopic curvature variation across the diffuse interface is obtained as

$$\frac{\mathrm{d}S}{\mathrm{d}\phi} = S_0 a\phi^{a-1}(1-\phi)^{b-1}\left(1-\frac{\phi}{\phi_\mathrm{c}}\right) \tag{12}$$

Since $\mathrm{d}S/\mathrm{d}\phi$ varies only across the diffuse interface, it must be interpreted as the local curvature of the microscopic interface after subtracting out the average curvature $\overline{\kappa}$ (such that it is macroscopically flat), i.e., $(\kappa - \overline{\kappa})$, as illustrated in Fig. 3. Note from Eq. (12) that $\mathrm{d}S/\mathrm{d}\phi$ changes its sign at $\phi = \phi_\mathrm{c} = a/(a+b)$, which implies that the atomic scale interface morphology changes from convex to concave. Hence, Eq. (12) may provide additional insight into the choices for a and b [20].

4. Conservation equations for a diffuse interface

In this section, the derivation of the averaged mass and momentum conservation equations for each phase inside (and outside) the diffuse interface is described. According to the discussion in Section 2, both phases k are assumed to be fluids. If one of the phases is a solid, the derivations do not apply to that phase, unless it is modeled as a fluid of infinite viscosity. Additional detail on some of the derivations can be found in Ref. [18], but none of the previous theories consider both surface tension and phase-change. The reduction of the two-phase model to a mixture formulation is also discussed briefly.

4.1. Mass

The local mass conservation equation for each phase and the jump condition in a sharp interface formulation are given, respectively, by

$$\frac{\partial\rho}{\partial t} + \nabla\cdot(\rho\boldsymbol{u}) = 0 \quad \text{and} \quad ||\rho(\boldsymbol{u}-\boldsymbol{u}_\mathrm{i})\cdot\boldsymbol{n}|| = 0 \tag{13}$$

where ρ is the density, $\boldsymbol{u}$ the velocity, $||\cdot||$ denotes a jump across the interface of a function f as $||f|| = f_1 - f_2$, and $\boldsymbol{u}_\mathrm{i}$ is the velocity of the interface between the two phases. Multiplying the local continuity equation by X_k and averaging yields the following averaged continuity equation for phase k [18]

$$\frac{\partial(\phi_k\rho_k)}{\partial t} + \nabla\cdot(\phi_k\rho_k\overline{\boldsymbol{u}}_k) = \Gamma_k. \tag{14}$$

For simplicity, both phases k are assumed microscopically incompressible. In Eq. (14), the average velocity of phase k is defined as $\overline{\boldsymbol{u}}_k = \langle X_k\boldsymbol{u}\rangle/\phi_k$ and the interfacial mass transfer rate per unit volume due to phase-change as $\Gamma_k = \langle[\rho(\boldsymbol{u}-\boldsymbol{u}_\mathrm{i})]^k\cdot\nabla X_k\rangle$. Multiplying the jump condition for mass by $|\nabla X_1|$ and averaging, results in the following averaged interfacial mass balance

$$\Gamma_1 + \Gamma_2 = 0. \tag{15}$$

Defining a mixture density as $\overline{\rho} = \rho_1\phi_1 + \rho_2\phi_2$ and a mass-averaged mixture velocity as $\overline{\boldsymbol{u}} = [\rho_1\phi_1\overline{\boldsymbol{u}}_1 + \rho_2\phi_2\overline{\boldsymbol{u}}_2]/\overline{\rho}$, Eqs. (14) and (15) can be combined to yield the following mixture continuity equation

$$\frac{\partial\overline{\rho}}{\partial t} + \nabla\cdot(\overline{\rho}\overline{\boldsymbol{u}}) = 0. \tag{16}$$

Eq. (16) is valid even for unequal phase velocities, and shows that the mixture is compressible inside the diffuse interface if the densities of the two phases are different. However, its main use would be in cases where the phase velocities can be assumed to be equal, i.e., $\bar{\boldsymbol{u}}_1 = \bar{\boldsymbol{u}}_2 = \bar{\boldsymbol{u}}$. In that case, and with the additional assumption that ρ_1 and ρ_2 are constant (but $\rho_1 \neq \rho_2$), additional insight can be gained by rewriting the averaged continuity equations as

$$\nabla \cdot \bar{\boldsymbol{u}} = \Gamma_1 \left(\frac{1}{\rho_1} - \frac{1}{\rho_2} \right) \quad \text{and} \quad \frac{\partial \phi}{\partial t} + \bar{\boldsymbol{u}} \cdot \nabla \phi = \Gamma_1 \left(\frac{1-\phi}{\rho_1} + \frac{\phi}{\rho_2} \right), \quad \text{for } \bar{\boldsymbol{u}}_1 = \bar{\boldsymbol{u}}_2 = \bar{\boldsymbol{u}}. \tag{17}$$

Eq. (17) show that in the absence of phase-change ($\Gamma_1 = 0$) the velocity field is solenoidal and the phase fraction ϕ is simply advected with $\bar{\boldsymbol{u}}$, even if $\rho_1 \neq \rho_2$. In the presence of phase-change ($\Gamma_1 \neq 0$) but for equal phase densities ($\rho_1 = \rho_2$), the velocity field is still solenoidal and the phase fraction ϕ is not only advected with $\bar{\boldsymbol{u}}$ but also changes with Γ_1, as expected. It is clear that in the presence of phase-change a separate model for Γ_1 needs to be supplied (e.g., the phase-field equation [1,3,10,12]).

4.2. Momentum

The local momentum conservation equation for each phase and the momentum jump condition at the interface can be written, respectively, as

$$\frac{\partial(\rho \boldsymbol{u})}{\partial t} + \nabla \cdot (\rho \boldsymbol{u}\boldsymbol{u}) = \nabla \cdot (-p\boldsymbol{I} + \boldsymbol{\tau}) + \rho \boldsymbol{g} \quad \text{and} \quad ||\rho \boldsymbol{u}(\boldsymbol{u} - \boldsymbol{u}_\mathrm{i}) \cdot \boldsymbol{n} - (-p\boldsymbol{I} + \boldsymbol{\tau}) \cdot \boldsymbol{n}|| = \sigma \kappa \boldsymbol{n} \tag{18}$$

where p is the pressure, $\boldsymbol{I}$ denotes the unit tensor, $\boldsymbol{\tau}$ the shear stress tensor, $\boldsymbol{g}$ the gravitational acceleration, and σ is the surface tension between the two phases. The surface tension is assumed constant and variations along the interface are not considered.

The averaged momentum equation for phase k is obtained by multiplying the first of Eq. (18) by X_k and averaging, to yield

$$\frac{\partial}{\partial t} \langle X_k \rho \boldsymbol{u} \rangle + \nabla \cdot \langle X_k \rho \boldsymbol{u}\boldsymbol{u} \rangle = -\nabla \langle X_k p \rangle + \nabla \cdot \langle X_k \boldsymbol{\tau} \rangle + \langle X_k \rho \boldsymbol{g} \rangle + \langle [\rho \boldsymbol{u}(\boldsymbol{u} - \boldsymbol{u}_\mathrm{i}) + (p\boldsymbol{I} - \boldsymbol{\tau})]^k \cdot \nabla X_k \rangle. \tag{19}$$

The term $\langle [p\boldsymbol{I}]^k \cdot \nabla X_k \rangle$ is split into two parts, with one representing the average interfacial pressure and the other accounting for unbalanced pressures at the interface, as

$$\langle [p\boldsymbol{I}]^k \cdot \nabla X_k \rangle = \bar{p}_{k,\mathrm{i}} \nabla \phi_k + \langle [(p - \bar{p}_{k,\mathrm{i}})\boldsymbol{I}]^k \cdot \nabla X_k \rangle \tag{20}$$

where the average interfacial pressure is defined as $\bar{p}_{k,\mathrm{i}} = \langle p|\nabla X_k| \rangle / |\nabla \phi|$ [19]. It may be argued that the value of $\bar{p}_{k,\mathrm{i}}$ is arbitrary in Eq. (20) (since it is added and subtracted back out); however, the above definition represents a physically meaningful choice. Assuming instantaneous microscopic pressure equilibrium [18,23], $\bar{p}_{k,\mathrm{i}}$ can be taken equal to the phase-averaged pressure of phase k, defined as $\bar{p}_k = \langle X_k p \rangle / \phi_k$, i.e.

$$\bar{p}_{k,\mathrm{i}} = \bar{p}_k. \tag{21}$$

Drew and Passman [19] suggest that for a fluid (or continuous) phase the difference between $\bar{p}_{k,\mathrm{i}}$ and $\bar{p}_k$ is proportional to the square of the slip velocity between the phases. Since the slip velocity inside the diffuse interface is assumed to be small (see Section 1) Eq. (21) can be expected to be a reasonable approximation. Other causes for a difference between the two pressures in large-scale two-phase flows, such as contact pressures and collisions between solid particles [19], are not relevant to the present system.

Neglecting the dispersive flux arising from the average of the $\boldsymbol{uu}$ product (see Section 1), the averaged momentum equation for phase k can now be written in the following final form

$$\frac{\partial}{\partial t}(\phi_k \rho_k \bar{\boldsymbol{u}}_k) + \nabla \cdot (\phi_k \rho_k \bar{\boldsymbol{u}}_k \bar{\boldsymbol{u}}_k) = -\phi_k \nabla \bar{p}_k + \nabla \cdot (\phi_k \bar{\boldsymbol{\tau}}_k) + \phi_k \rho_k \boldsymbol{g} + \Gamma_k \bar{\boldsymbol{u}}_{k,\Gamma} + \boldsymbol{M}_k \tag{22}$$

where $\bar{\boldsymbol{\tau}}_k = \langle X_k \boldsymbol{\tau} \rangle / \phi_k$, $\boldsymbol{M}_k$ is the interfacial force density of phase k, and $\bar{\boldsymbol{u}}_{k,\Gamma} = \langle [\rho \boldsymbol{u}(\boldsymbol{u} - \boldsymbol{u}_\mathrm{i})]^k \cdot \nabla X_k \rangle / \Gamma_k$. The latter expression defines an average normal interfacial velocity of phase k due to phase-change. The modeling of the average shear stress, $\bar{\boldsymbol{\tau}}_k$, is discussed in Section 5. In the absence of flow and surface tension Eq. (22) reduces to $\nabla \bar{p}_k = \rho_k \boldsymbol{g}$, as one would expect for a fluid.

The averaging process yields the following expression for the interfacial force density, $\boldsymbol{M}_k$, in Eq. (22)

$$\boldsymbol{M}_k = \langle [(p_k - \bar{p}_k)\boldsymbol{I}] \cdot \nabla X_k \rangle - \langle \boldsymbol{\tau}_k \cdot \nabla X_k \rangle. \tag{23}$$

This term represents unbalanced pressures and shear stresses at the interface. For large-scale two-phase systems, it accounts for the interfacial forces on phase k due to shear and form drag, as well as unbalanced pressures leading to lift or virtual mass effects [18]. In the present context of diffuse interface modeling, the physical meaning of such forces is not immediately clear. However, a simple model for the viscous contribution to the interfacial force density, assuming a small slip velocity inside the diffuse interface, is presented in Section 7. It is also shown in Section 7 that the interfacial force density includes a new contribution due to unbalanced pressures that are caused by curvature variations in the presence of surface tension.

The averaged interfacial momentum balance, obtained by averaging the second of Eq. (18) after multiplying it by $|\nabla X_1|$, is given by

$$\Gamma_1 \bar{\boldsymbol{u}}_{1,\Gamma} + \bar{p}_1 \nabla \phi_1 + \boldsymbol{M}_1 + \Gamma_2 \bar{\boldsymbol{u}}_{2,\Gamma} + \bar{p}_2 \nabla \phi_2 + \boldsymbol{M}_2 = \boldsymbol{M}_\mathrm{i} = \sigma \langle \kappa \nabla X_1 \rangle \tag{24}$$

where $\boldsymbol{M}_\mathrm{i}$ is the averaged interfacial momentum source due to surface tension. The term $\langle \kappa \nabla X_1 \rangle$ cannot simply be modeled as $\bar{\kappa} \nabla \phi$, because that would violate the definition of the average curvature given by Eq. (7). To overcome this problem, the same splitting strategy as for the term $\langle [p\boldsymbol{I}]^k \cdot \nabla X_k \rangle$ (see Eq. (20)) is applied to $\boldsymbol{M}_\mathrm{i}$ to yield

$$\boldsymbol{M}_\mathrm{i} = \sigma \bar{\kappa} \nabla \phi + \sigma \langle (\kappa - \bar{\kappa}) \nabla X_1 \rangle \tag{25}$$

where the first term represents a contribution from the average curvature of the interface and the second term is a contribution from microscopic curvatures inside the diffuse interface that is present even if $\bar{\kappa} = 0$ (see Section 3). A model for the second term is provided in Section 6.

Additional insight into the interfacial momentum balance can be gained by splitting it into the components tangential and normal to the diffuse interface. In the tangential direction (i.e., along contours of constant ϕ), Eq. (24) becomes

$$\boldsymbol{M}_{1,\mathrm{t}} + \boldsymbol{M}_{2,\mathrm{t}} = 0 \tag{26}$$

where $\boldsymbol{M}_{1,\mathrm{t}}$ and $\boldsymbol{M}_{2,\mathrm{t}}$ are the tangential components of the interfacial force density of the two phases. Eq. (26) indicates that, in the absence of surface tension variations along the interface (i.e., the Marangoni effect), as assumed in the present study, the tangential components of the interfacial force densities balance each other [19]. In the direction normal to the diffuse interface Eq. (24) can be written as

$$\bar{p}_1 - \bar{p}_2 = \frac{\boldsymbol{M}_\mathrm{i} \cdot \nabla \phi}{|\nabla \phi|^2} + \frac{\Gamma_2 (\bar{\boldsymbol{u}}_{1,\Gamma} - \bar{\boldsymbol{u}}_{2,\Gamma}) \cdot \nabla \phi}{|\nabla \phi|^2} - \frac{(\boldsymbol{M}_1 + \boldsymbol{M}_2) \cdot \nabla \phi}{|\nabla \phi|^2} \tag{27}$$

It can be seen from Eq. (27) that the difference in the average pressures between the phases is due to the effect of surface tension, the contraction or expansion flow induced by phase-change and a density difference, and any difference in the magnitude of the interfacial force densities of the phases in the $\nabla \phi$ direction. Almost all previous studies of large-scale two-phase flows [18,19,21] assume that the normal components of the interfacial force densities

of the two phases balance each other. Only Bercovici et al. [20], in a study of compaction and damage of a two-phase mixture, identify a pressure difference between the phases due to unbalanced interfacial shear stresses in the normal direction. In the present study on diffuse interface modeling, such an imbalance is not considered and the last term in Eq. (27) is assumed to vanish. In view of the above discussion, the interfacial force density, $\boldsymbol{M}_k$, acts equally and oppositely between the phases in both directions, i.e.

$$\boldsymbol{M}_1 = -\boldsymbol{M}_2. \tag{28}$$

Eq. (28) implies that the interfacial force density is recognized as a force of one phase against the other, and not as a force of either phase against the interface [20]. Note that in view of Eq. (28) the interfacial force densities in the averaged interfacial momentum balance, Eq. (24), cancel each other.

The averaged mixture momentum equation is obtained by adding up Eq. (22) for each phase and making use of Eq. (24), to yield

$$\frac{\partial}{\partial t}(\overline{\rho}\overline{\boldsymbol{u}}) + \nabla\cdot(\overline{\rho}\overline{\boldsymbol{u}}\overline{\boldsymbol{u}}) = -\nabla\overline{p} + \nabla\cdot\overline{\boldsymbol{\tau}} + \overline{\rho}\boldsymbol{g} + \boldsymbol{M}_\mathrm{i} - \nabla\cdot\left[\frac{\phi(1-\phi)(\overline{\boldsymbol{u}}_1 - \overline{\boldsymbol{u}}_2)(\overline{\boldsymbol{u}}_1 - \overline{\boldsymbol{u}}_2)\rho_1\rho_2}{\overline{\rho}}\right] \tag{29}$$

where the mixture pressure and the mixture shear stress are defined, respectively, as $\overline{p} = \phi_1\overline{p}_1 + \phi_2\overline{p}_2$ and $\overline{\boldsymbol{\tau}} = \phi_1\overline{\boldsymbol{\tau}}_1 + \phi_2\overline{\boldsymbol{\tau}}_2$. Again, the main use of Eq. (29) would be in Case III, where the velocities of the two phases can be assumed to be equal inside the diffuse interface. Then, the last term in Eq. (29) vanishes and Eq. (29) is identical to the thermodynamically derived momentum equation in Ref. [12].

The remaining un-modeled terms in the averaged momentum equations are: the average shear stress, $\overline{\boldsymbol{\tau}}_k$; the average interfacial momentum source due to surface tension, $\boldsymbol{M}_\mathrm{i}$ (in particular, the second term on the right hand side of Eq. (25)); and the interfacial force density, $\boldsymbol{M}_k$. Models for these three terms are proposed in the following sections.

5. Modeling of the average shear stress

A model for the average shear stress of phase k is obtained by starting with the following constitutive relation for the local shear stress in a Newtonian fluid

$$\boldsymbol{\tau} = \mu\left(\nabla\boldsymbol{u} + \nabla\boldsymbol{u}^\mathrm{T} - \frac{2}{3}(\nabla\cdot\boldsymbol{u})\boldsymbol{I}\right) \tag{30}$$

where μ is the viscosity and the factor $-2/3$ is due to Stoke's assumption [30]. Averaging Eq. (30) results in

$$\begin{aligned}
\phi_k\overline{\boldsymbol{\tau}}_k &= \left\langle X_k\mu_k\left(\nabla\boldsymbol{u} + \nabla\boldsymbol{u}^\mathrm{T} - \frac{2}{3}(\nabla\cdot\boldsymbol{u})\boldsymbol{I}\right)\right\rangle \\
&= \mu_k\left\langle\nabla(X_k\boldsymbol{u}) + \nabla(X_k\boldsymbol{u})^\mathrm{T} - \frac{2}{3}\nabla\cdot(X_k\boldsymbol{u})\boldsymbol{I} - \boldsymbol{u}\nabla X_k - \nabla X_k\boldsymbol{u} + \frac{2}{3}(\boldsymbol{u}\cdot\nabla X_k)\boldsymbol{I}\right\rangle \\
&= \mu_k^*\left[\nabla(\phi_k\overline{\boldsymbol{u}}_k) + \nabla(\phi_k\overline{\boldsymbol{u}}_k)^\mathrm{T} - \frac{2}{3}\nabla\cdot(\phi_k\overline{\boldsymbol{u}}_k)\boldsymbol{I} - \overline{\boldsymbol{u}}_{k,\mathrm{i}}\nabla\phi_k - \nabla\phi_k\overline{\boldsymbol{u}}_{k,\mathrm{i}} + \frac{2}{3}(\overline{\boldsymbol{u}}_{k,\mathrm{i}}\cdot\nabla\phi_k)\boldsymbol{I}\right]
\end{aligned} \tag{31}$$

where μ_k^* is an effective viscosity of phase k. In Eq. (31), the average interfacial velocity of phase k, $\overline{\boldsymbol{u}}_{k,\mathrm{i}}$, is defined as

$$\overline{\boldsymbol{u}}_{k,\mathrm{i}} = \frac{\langle\boldsymbol{u}|\nabla X_k|\rangle}{|\nabla\phi|}. \tag{32}$$

Note that $\overline{\boldsymbol{u}}_{k,\mathrm{i}}$ is defined differently from the interfacial velocity $\overline{\boldsymbol{u}}_{k,\Gamma} = \langle[\rho\boldsymbol{u}(\boldsymbol{u}-\boldsymbol{u}_\mathrm{i})]^k\cdot\nabla X_k\rangle/\Gamma_k$ introduced in Section 4 in connection with phase-change. Eq. (32) defines an average interfacial velocity that includes all

components in the averaging process, while the definition for $\bar{\boldsymbol{u}}_{k,\Gamma}$ only collects the component normal to the microscopic interface during averaging and is non-zero only in the presence of phase-change. The last equality in Eq. (31) is based on a method similar to the one used in Ref. [23] and requires some explanation. The term $\langle \boldsymbol{u} \nabla X_k \rangle$ is split into $\langle \boldsymbol{u} \nabla X_k \rangle = \bar{\boldsymbol{u}}_{k,\mathrm{i}} \nabla \phi + \langle (\boldsymbol{u} - \bar{\boldsymbol{u}}_{k,\mathrm{i}}) \nabla X_k \rangle$, following the same strategy as for the terms $\langle p \nabla X_k \rangle$ and $\langle \kappa \nabla X_k \rangle$ in Section 4. The term $\langle (\boldsymbol{u} - \bar{\boldsymbol{u}}_{k,\mathrm{i}}) \nabla X_k \rangle$, representing the average of local interfacial velocity fluctuations, is then "absorbed" into an effective viscosity, μ_k^*, as shown in Eq. (31) [23]. However, in the following μ_k^* is simply taken equal to the actual fluid viscosity, i.e., $\mu_k^* = \mu_k$. This simplification can only be viewed as a first approximation for the two-phase flow inside a diffuse interface.

The last portion of Eq. (31) can be rewritten in the following, more transparent form

$$\phi_k \bar{\boldsymbol{\tau}}_k = \mu_k \phi_k \left(\nabla \bar{\boldsymbol{u}}_k + \nabla \bar{\boldsymbol{u}}_k^{\mathrm{T}} - \frac{2}{3} (\nabla \cdot \bar{\boldsymbol{u}}_k) \boldsymbol{I} \right) + \mu_k \left[\nabla \phi_k (\bar{\boldsymbol{u}}_k - \bar{\boldsymbol{u}}_{k,\mathrm{i}}) + (\bar{\boldsymbol{u}}_k - \bar{\boldsymbol{u}}_{k,\mathrm{i}}) \nabla \phi_k - \frac{2}{3} \nabla \phi \cdot (\bar{\boldsymbol{u}}_k - \bar{\boldsymbol{u}}_{k,\mathrm{i}}) \boldsymbol{I} \right] \tag{33}$$

The first part on the right-hand-side of Eq. (33) accounts for the viscous stress of phase k to itself as in a single phase system. The second part represents the contribution to the average viscous stress of phase k due to relative motion between the two phases. This part is proportional to the difference between the phase-averaged and interfacial velocities, $(\bar{\boldsymbol{u}}_k - \bar{\boldsymbol{u}}_{k,\mathrm{i}})$, and to $\nabla \phi_k$, indicating that it is non-zero only inside the diffuse interface.

A simple but practical expression for $\bar{\boldsymbol{u}}_{k,\mathrm{i}}$ is obtained by assuming that $\bar{\boldsymbol{u}}_{k,\mathrm{i}}$ is a viscosity weighted linear function of the average velocities of both phases, i.e.

$$\bar{\boldsymbol{u}}_{k,\mathrm{i}} = \frac{\mu_1 \phi_2 \bar{\boldsymbol{u}}_1 + \mu_2 \phi_1 \bar{\boldsymbol{u}}_2}{\mu_1 \phi_2 + \mu_2 \phi_1}. \tag{34}$$

This concept is schematically illustrated in Fig. 4 for a simple shear flow inside a small unit cell. The microscopic velocity profile is continuous at the interface between the two phases. For equal viscosities of the two phases, the interfacial velocity can be seen from Fig. 4a to be given by $\bar{\boldsymbol{u}}_{k,\mathrm{i}} = \phi_2 \bar{\boldsymbol{u}}_1 + \phi_1 \bar{\boldsymbol{u}}_2$. For unequal viscosities (Fig. 4b), Eq. (34) results. Note that Eq. (34) provides an average interfacial velocity that is independent of the phase, i.e., $\bar{\boldsymbol{u}}_{1,\mathrm{i}} = \bar{\boldsymbol{u}}_{2,\mathrm{i}}$. This symmetry is necessary for modeling a system where the two fluids are in principle interchangeable. The statement $\bar{\boldsymbol{u}}_{1,\mathrm{i}} = \bar{\boldsymbol{u}}_{2,\mathrm{i}}$ can simply be interpreted as an averaged no-slip condition at the interface between the two phases. One could argue that the symmetry is broken in the presence of phase-change when the two phases have a different density and $\bar{\boldsymbol{u}}_{1,\Gamma} \neq \bar{\boldsymbol{u}}_{2,\Gamma}$ (see Eq. (27)). However, as mentioned above, the definitions of $\bar{\boldsymbol{u}}_{k,\mathrm{i}}$ and $\bar{\boldsymbol{u}}_{k,\Gamma}$ are quite different, and Eq. (34) can be expected to be a good approximation even when $\bar{\boldsymbol{u}}_{1,\Gamma} \neq \bar{\boldsymbol{u}}_{2,\Gamma}$. For a two-phase system where phase 1 is a solid that is modeled as a fluid with a large viscosity [12], Eq. (34) yields $\bar{\boldsymbol{u}}_{2,\mathrm{i}} = \bar{\boldsymbol{u}}_1$ in the limit of $\mu_1 \gg \mu_2$, which is like a no-slip condition on a rigid body moving with velocity $\bar{\boldsymbol{u}}_1$.

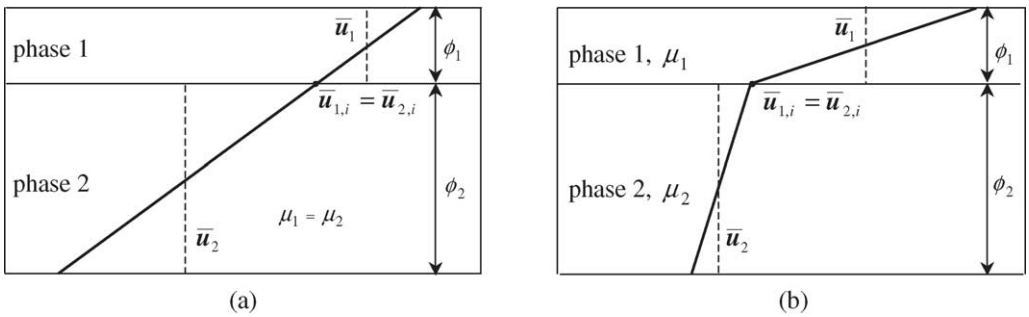

Fig. 4. Schematic illustration of the microscopic velocity profile (heavy solid line) inside a unit cell for a simple shear flow with (a) identical and (b) different viscosities.

Substituting Eq. (34) into Eq. (33), yields the following final expression for the average shear stress of phase k

$$\phi_k \overline{\boldsymbol{\tau}}_k = \mu_k \phi_k \left(\nabla \overline{\boldsymbol{u}}_k + \nabla \overline{\boldsymbol{u}}_k^{\mathrm{T}} - \frac{2}{3} (\nabla \cdot \overline{\boldsymbol{u}}_k) \boldsymbol{I} \right) + \frac{\mu_j \mu_k \phi_k}{\mu_k \phi_j + \mu_j \phi_k} \left[\nabla \phi_k (\overline{\boldsymbol{u}}_k - \overline{\boldsymbol{u}}_j) + (\overline{\boldsymbol{u}}_k - \overline{\boldsymbol{u}}_j) \nabla \phi_k - \frac{2}{3} \nabla \phi \cdot (\overline{\boldsymbol{u}}_k - \overline{\boldsymbol{u}}_j) \boldsymbol{I} \right]. \tag{35}$$

where the subscript j denotes the other phase in a two-phase system. Eq. (35) provides a constitutive equation for the average shear stress in terms of the velocities of both phases. Drew and Passman [19] also introduced a model for $\overline{\boldsymbol{\tau}}_k$ that involves the velocities of both phases. The model in Ref. [19], however, introduces several different effective viscosities that are highly case dependent and generally unknown. The present model avoids that complication. In Appendix A, Eq. (35) is examined further by applying it to the limiting cases discussed in Section 2 and illustrated in Fig. 1.

6. Modeling of the interfacial momentum source term

The averaged interfacial momentum source is given by Eq. (25) as $\boldsymbol{M}_{\mathrm{i}} = \sigma \overline{\kappa} \nabla \phi + \sigma \langle (\kappa - \overline{\kappa}) \nabla X_1 \rangle$, where $\langle (\kappa - \overline{\kappa}) \nabla X_1 \rangle$ represents the mean effect of microscopic curvatures inside the diffuse interface that remains even if the average curvature $\overline{\kappa}$ vanishes. This term can be modeled by considering the previous discussion on superposition of microscopic and macroscopic interface morphologies and Fig. 3. In Section 3, the term $\mathrm{d}S/\mathrm{d}\phi$ was identified as a microscopic curvature inside a flat diffuse interface. Hence, the following model for $\langle (\kappa - \overline{\kappa}) \nabla X_1 \rangle$ is proposed here:

$$\langle (\kappa - \overline{\kappa}) \nabla X_1 \rangle = -\frac{\mathrm{d}S}{\mathrm{d}\phi} \nabla \phi. \tag{36}$$

The negative sign ensures that $\langle (\kappa - \overline{\kappa}) \nabla X_1 \rangle$ is positive for $\phi < \phi_{\mathrm{c}}$. Eq. (36) may not appear as a generally valid model for $\langle (\kappa - \overline{\kappa}) \nabla X_1 \rangle$ because this term is a vector [18]. However, this does not represent a problem because the microscopic curvature varies only in the normal direction across the diffuse interface. Substituting Eq. (36) into Eq. (25) yields

$$\boldsymbol{M}_{\mathrm{i}} = \sigma \left(\overline{\kappa} - \frac{\mathrm{d}S}{\mathrm{d}\phi} \right) \nabla \phi \tag{37}$$

which illustrates that $\boldsymbol{M}_{\mathrm{i}}$ remains even for a macroscopically flat interface ($\overline{\kappa} = 0$) because of the presence of microscopic curvatures inside the diffuse interface. Substituting Eq. (11) for $\overline{\kappa}$ into Eq. (37) gives

$$\boldsymbol{M}_{\mathrm{i}} = -\frac{\sigma}{S} \nabla^2 \phi \nabla \phi \tag{38}$$

which is the main result of the present section.

Before proceeding, the present expression for the interfacial momentum source term given by Eq. (38) is compared to the corresponding term obtained from thermodynamic or gradient theories for diffuse interfaces. In these theories, a capillary stress tensor is introduced as $\boldsymbol{m} = \sigma l_{\mathrm{i}} (|\nabla \phi|^2 \boldsymbol{I}/2 - \nabla \phi \otimes \nabla \phi)$ [12], where l_{i} is the interface width as before. The interfacial momentum source term is related to the capillary stress tensor through $\boldsymbol{M}_{\mathrm{i}}^{\mathrm{cs}} = \nabla \cdot \boldsymbol{m}$, where the superscript cs denotes that it corresponds to the capillary stress tensor. Hence

$$\boldsymbol{M}_{\mathrm{i}}^{\mathrm{cs}} = -\sigma l_{\mathrm{i}} \nabla^2 \phi \nabla \phi. \tag{39}$$

It can be seen that Eqs. (38) and (39) are virtually identical, since $S \sim 1/l_{\mathrm{i}}$. This lends considerable confidence to the present derivation. The only difference between $\boldsymbol{M}_{\mathrm{i}}$ and $\boldsymbol{M}_{\mathrm{i}}^{\mathrm{cs}}$ is that S is a function of ϕ, according to Eq. (8), whereas

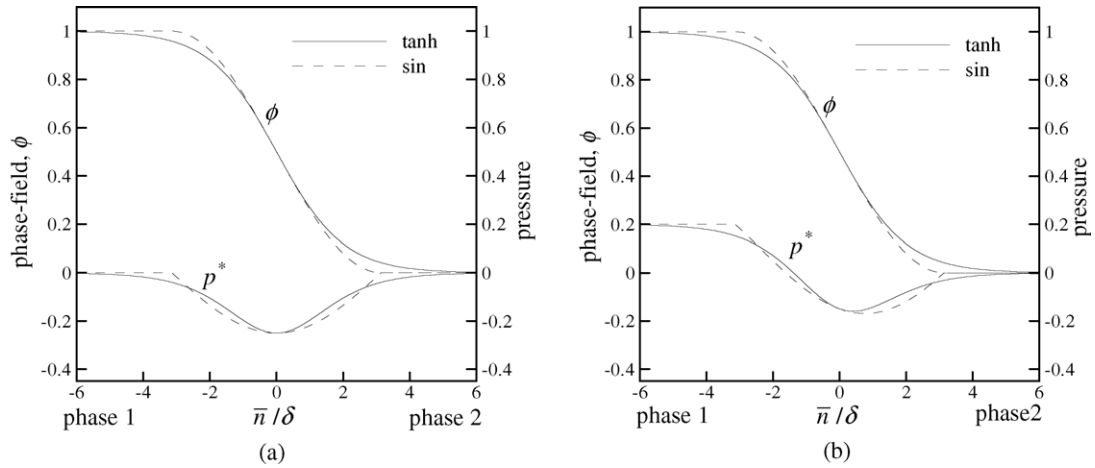

Fig. 5. Variation of the phase-field profile and the mixture pressure across (a) planar and (b) spherical (with $R/\delta = 10$) interfaces in equilibrium; results are shown for two different profiles: $\phi = [1 - \tanh(\overline{n}/2\delta)]/2$ and $\phi = [1 - \sin(\overline{n}/2\delta)]/2$.

l_i is a constant. Substituting, for example, the hyperbolic tangent profile for ϕ (with $a = b = 1$ and $S_0 = 1/\delta$), Eqs. (38) and (39) become, respectively: $M_\mathrm{i} = \sigma\phi(1-\phi)(1-2\phi)/\delta^2$ and $\boldsymbol{M}_\mathrm{i}^\mathrm{cs} = 6\sigma\phi^2(1-\phi)^2(1-2\phi)/\delta^2$ (since $l_\mathrm{i} = 6\delta$ for the hyperbolic tangent profile) in the direction normal to the interface. It can be seen that the two expressions are very similar and have minima and maxima that differ only in magnitude. Since different potentials can be used in the thermodynamic approach (resulting in different ϕ profiles), and other choices for a and b can be used for S as discussed in Section 3, it can be said that the difference between $\boldsymbol{M}_\mathrm{i}$ and $\boldsymbol{M}_\mathrm{i}^\mathrm{cs}$ is generally insignificant.

Further insight into the interfacial momentum source term can be gained by considering an interface in equilibrium without flow and gravity. The mixture momentum equation, Eq. (29), then becomes $\nabla\overline{p} = -\sigma/S\nabla^2\phi\nabla\phi$ which can be solved for the mixture pressure $\overline{p}$. For example, for a macroscopically planar interface ($\overline{\kappa} = 0$) the solution is given by $\overline{p} = \overline{p}_{2,\infty} - \sigma S_0\phi^a(1-\phi)^b$, and for a macroscopically spherical interface of radius R ($\overline{\kappa} = 2/R$) it is $\overline{p} = \overline{p}_{2,\infty} + \sigma\overline{\kappa}\phi - \sigma S_0\phi^a(1-\phi)^b$, where $\overline{p}_{2,\infty}$ is a reference pressure far from the interface in phase 2. Results in terms of the dimensionless mixture pressure $p^* = (\overline{p} - \overline{p}_{2,\infty})/(\sigma/\delta)$ are shown in Fig. 5a and b for planar and spherical diffuse interfaces, respectively. Pressure profiles across the diffuse interface are plotted in Fig. 5 for the following choices of the constants in Eq. (8): (i) $a = b = 1$ and $S_0 = 1/\delta$, which corresponds to the hyperbolic tangent ϕ profile, and (ii) $a = b = 1/2$ and $S_0 = 1/(2\delta)$, which gives the sinusoidal ϕ profile. It can be seen that the differences in the results for the two ϕ profiles are small. For a planar interface, the far-field pressures are identical, i.e., $\overline{p}_{1,\infty} = \overline{p}_{2,\infty}$, as expected. Inside the diffuse interface a pressure "hump" of depth $\Delta p^* = 0.25$ at $\phi = 0.5$ can be observed that is a manifestation of the capillary stress. If the two phases are fluids, this pressure hump would act to keep the fluids from mixing. For the spherical interface, the minimum in the hump is shifted to $\phi = 0.5 - \delta/R$ and the difference between the far field pressures is equal to $\overline{p}_{1,\infty} - \overline{p}_{2,\infty} = 2\sigma/R$, as expected from the Young–Laplace equation for a sharp interface. These simple examples illustrate that, as opposed to the commonly used continuum surface force (CSF) expression $\boldsymbol{M}_\mathrm{i}^\mathrm{CSF} = \sigma\overline{\kappa}\nabla\phi$ [2], the present interfacial momentum source term accounts for immiscibility between the phases due to surface tension.

7. Modeling of the interfacial force density

Another important aspect of the present study is the modeling of the interfacial force density of phase k, $\boldsymbol{M}_k$, in the context of a diffuse interface approach. This term is essential for a two-phase model because the interactions between the phases must be explicitly accounted for. As discussed in Section 4, $\boldsymbol{M}_k$ represents the interfacial force

density due to unbalanced pressures and stresses at the interface and acts equally but oppositely between the phases. As shown in the following, the interfacial force density includes two contributions: (1) unbalanced pressures due to curvature variations in the presence of surface tension; this part is non-zero even in the absence of flow; and (2) dissipative (viscous) drag due to relative motion between the phases.

First, consider a case without flow and gravity. The momentum equations for the two phases, based on Eq. (22), become $\phi_1 \nabla \bar{p}_1 = \boldsymbol{M}_1^\sigma$ and $\phi_2 \nabla \bar{p}_2 = \boldsymbol{M}_2^\sigma$. Using Eq. (37), Eq. (27) becomes $\bar{p}_1 - \bar{p}_2 = \sigma(\bar{\kappa} - \mathrm{d}S/\mathrm{d}\phi)$ (this is not a difference between far-field pressures, but between the pressures of the two phases inside the diffuse interface). Since $\boldsymbol{M}_1 = -\boldsymbol{M}_2$, the previous equations can be solved for the interfacial force densities of each phase to yield $\boldsymbol{M}_1^\sigma = \sigma\phi(1-\phi)\nabla(\bar{\kappa} - \mathrm{d}S/\mathrm{d}\phi)$ and $\boldsymbol{M}_2^\sigma = -\sigma\phi(1-\phi)\nabla(\bar{\kappa} - \mathrm{d}S/\mathrm{d}\phi)$. Since the curvature changes its sign to a switch of the phases, $\boldsymbol{M}_k^\sigma$ can be rewritten in a phase-invariant form as

$$\boldsymbol{M}_k^\sigma = \sigma\phi_k\phi_j\nabla\left(\bar{\kappa}_k - \frac{\mathrm{d}S}{\mathrm{d}\phi_k}\right) \tag{40}$$

where $\bar{\kappa}_k$ is the average curvature of phase k, which for phases 1 and 2 is $\bar{\kappa}_1 = \bar{\kappa}$ and $\bar{\kappa}_2 = -\bar{\kappa}$, respectively. Eq. (40) defines an interfacial force density in the absence of flow that has the effect of balancing the average and microscopic curvature variations of the diffuse interface in the presence of surface tension. The resulting variation of the pressures of the two phases across the diffuse interface, in the absence of flow and gravity, is presented in Appendix B.

Second, consider a case with flow but without surface tension. In the limit of Case II ($\bar{\boldsymbol{u}}_1 = 0$), and for the hyperbolic tangent ϕ profile ($a = b = 1$ and $S_0 = 1/\delta$ in Eq. (8)), Beckermann et al. [3] proposed the following model for the dissipative interfacial force density of phase 2

$$\boldsymbol{M}_2^\mathrm{d} = -\frac{\mu_2\phi h S}{\delta}\bar{\boldsymbol{u}}_2, \quad \text{for Case II.} \tag{41}$$

This expression is based on an analogy with slow flow through a rigid stationary porous medium and assumes that the drag on the fluid phase is linearly proportional to the average velocity, $\bar{\boldsymbol{u}}_2$, and the interfacial area per unit volume, $S = |\nabla\phi|$, and inversely proportional to the diffuse interface thickness. The dimensionless "friction" constant h was determined from an asymptotic analysis for plane shear flow past a diffuse interface. For the hyperbolic tangent ϕ profile across the diffuse interface, it was found that a value of $h = 2.757$ results in the shear velocity profile for a diffuse interface approaching that for a sharp interface with a no-slip condition at $\phi = 0.5$, as $\phi \to 0$ (i.e., in the fluid phase) [3]. This value for h holds regardless of the interface width, i.e., δ. Hence, in actual computations the interface width can be chosen artificially large, as long as it is much smaller than the macroscopic length l_c.

For the present case of two-phase flow inside the diffuse interface, Eq. (41) needs to be modified to (i) account for the motion of both phases, (ii) be phase-invariant, and (iii) be valid for any ϕ profile across the diffuse interface (i.e., any $a = b$ in Eq. (8) for S). First, Eq. (41) is rewritten as

$$\boldsymbol{M}_k^\mathrm{d} = -\frac{\mu_k\phi_k h S}{\delta}(\bar{\boldsymbol{u}}_k - \bar{\boldsymbol{u}}_{k,\mathrm{i}}). \tag{42}$$

Eq. (42) recognizes the fact that in two-phase flow the drag is proportional to the difference between the average and interfacial velocities of a phase (note that $\bar{\boldsymbol{u}}_{2,\mathrm{i}} = 0$ in Case II because $\bar{\boldsymbol{u}}_{1,\mathrm{i}} = \bar{\boldsymbol{u}}_{2,\mathrm{i}}$ and the solid is assumed rigid and stationary). Substituting the model for $\bar{\boldsymbol{u}}_{k,\mathrm{i}}$, given by Eq. (34), into Eq. (42) yields the following final, phase-invariant form of the dissipative interfacial force density of phase k

$$\boldsymbol{M}_k^\mathrm{d} = -\frac{\mu_k\mu_j}{\mu_k\phi_j + \phi_k\mu_j}\frac{\phi_k\phi_j h S}{\delta}(\bar{\boldsymbol{u}}_k - \bar{\boldsymbol{u}}_j) = -\alpha(\bar{\boldsymbol{u}}_k - \bar{\boldsymbol{u}}_j). \tag{43}$$

Now it can be seen that the drag is proportional to the relative velocity between the phases, as expected [19,20]. The pre-factor α is a function of the viscosities and volume fractions of both phases. It is shown in Section 8.1.1 that the same "friction" constant h as in Case II can be used for the general case of two-phase flow (Case I). While

the general form of Eq. (43) is believed to be valid for any choice of $a = b$, slightly different values for h result for different ϕ profiles. For example, for the sinusoidal profile ($a = b = 1/2$ and $S_0 = 1/(2\delta)$), it was found (not shown here for brevity) that $h = 2.5$, instead of the 2.757 value that must be used with the hyperbolic tangent ϕ profile ($a = b = 1$ and $S_0 = 1/\delta$). Again, the value of h is independent of the interface width, i.e., δ. The interfacial drag model given by Eq. (43) is illustrated further in Appendix C for a simple one-dimensional flow across a diffuse interface.

Based on the previous discussion, the total interfacial force density of phase k, $\boldsymbol{M}_k$, is simply taken as the sum of the interfacial forces due to curvature variations and due to viscous drag, i.e.

$$\boldsymbol{M}_k = \frac{\mu_k \mu_j}{\mu_k \phi_j + \phi_k \mu_j} \frac{\phi_k \phi_j h S}{\delta} (\bar{\boldsymbol{u}}_j - \bar{\boldsymbol{u}}_k) + \sigma \phi_j \phi_k \nabla \left(\bar{\kappa}_k - \frac{\mathrm{d}S}{\mathrm{d}\phi_k} \right). \tag{44}$$

All other effects are neglected. Note that Eq. (44) is completely symmetric with respect to the phases, i.e., $\boldsymbol{M}_1 = -\boldsymbol{M}_2$.

8. Examples

The model is tested for two simple one-dimensional two-phase flows involving a macroscopically flat interface: (i) a shear flow parallel to a diffuse interface and (ii) a flow normal to a diffuse interface that is driven by phase-change in the presence of a density difference between the phases. In all cases, the constants a and b in Eq. (8) are taken equal to unity and $S_0 = 1/\delta$, such that the interfacial area per unit volume, S, is given by

$$S = \frac{\phi(1-\phi)}{\delta} \tag{45}$$

Using Eq. (9), the phase-field profile across the diffuse interface (in the x-direction) is then given by

$$\phi = \frac{1}{2} \left[1 - \tanh \left(\frac{x}{2\delta} \right) \right]. \tag{46}$$

This profile is used even in the second example that involves phase-change, and no evolution equation for ϕ is solved.

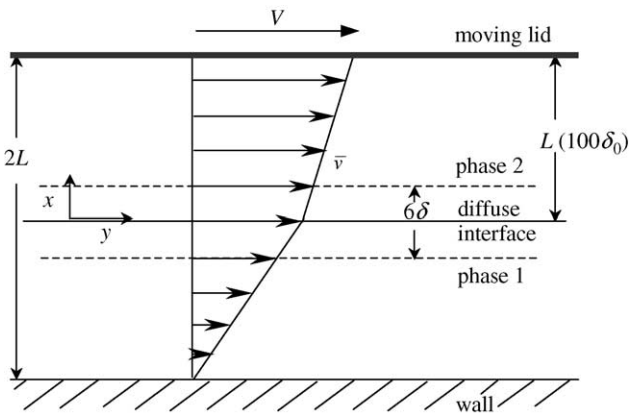

Fig. 6. Schematic illustration of the two-phase shear flow system.

8.1. Two-phase shear flow

The two-phase shear flow system considered in this example is illustrated in Fig. 6. A stationary interface, aligned with the y coordinate, is centered between two walls and separates two phases of different, but constant, viscosity and equal density. The wall at $x = -L$ is fixed and the wall at $x = L$ is moving with a constant speed V into the y-direction. The flow is assumed to be fully developed with no slip conditions at $x = \pm L$. For a sharp interface, the velocity profile is linear in each phase with the slopes determined directly by the viscosity ratio $r_\mu = \mu_1/\mu_2$ and the velocity of the interface in the y-direction given by $v_\mathrm{i} = V/(r_\mu + 1)$. The length L is taken as a constant equal to $100\delta_0$, where δ_0 is a reference value for δ (not to scale in Fig. 6 for illustration purposes).

8.1.1. Case I

For Case I, the y-momentum equations for phases 1 and 2 are given, respectively, by

$$0 = \mu_1 \frac{\mathrm{d}}{\mathrm{d}x}\left[\phi\frac{\mathrm{d}\bar{v}_1}{\mathrm{d}x} + \frac{\mathrm{d}\phi}{\mathrm{d}x}\frac{\mu_2\phi}{\mu_1(1-\phi)+\phi\mu_2}(\bar{v}_1 - \bar{v}_2)\right] - \frac{\mu_1\mu_2}{\mu_1(1-\phi)+\phi\mu_2}\frac{\phi(1-\phi)hS}{\delta}(\bar{v}_1 - \bar{v}_2). \tag{47}$$

$$0 = \mu_2 \frac{\mathrm{d}}{\mathrm{d}x}\left[(1-\phi)\frac{\mathrm{d}\bar{v}_2}{\mathrm{d}x} + \frac{\mathrm{d}\phi}{\mathrm{d}x}\frac{\mu_1(1-\phi)}{\mu_1(1-\phi)+\phi\mu_2}(\bar{v}_1 - \bar{v}_2)\right] + \frac{\mu_1\mu_2}{\mu_1(1-\phi)+\phi\mu_2}\frac{\phi(1-\phi)hS}{\delta}(\bar{v}_1 - \bar{v}_2). \tag{48}$$

where $\bar{v}_k$ is the velocity of phase k in the y-direction. The above highly coupled equations are solved numerically for the phase velocities $\bar{v}_1$ and $\bar{v}_2$. To ease the computations, Eqs. (47) and (48) can be combined and rewritten in terms of the mixture velocity $\bar{v} = \phi_1\bar{v}_1 + \phi_2\bar{v}_2$ and the slip velocity $\Delta\bar{v} = \bar{v}_1 - \bar{v}_2$ (the resulting equations are omitted here for brevity). The advantage of solving the momentum equations in terms of these two velocities is that they are well defined even for $\phi_k \to 0$.

Calculated velocity profiles are shown in Fig. 7a–c for viscosity ratios, $r_\mu = \mu_1/\mu_2$, of 1, 10, and 10^3, respectively (in the actual computations, μ_1 was changed while μ_2 was held constant). In each figure, results are presented for $\delta = \delta_0$, $5\delta_0$, and $10\delta_0$. The upper panels show the profiles for the phase-field and the mixture velocity $\bar{v}$, while the lower panels provide the individual phase velocity profiles, $\bar{v}_1$ and $\bar{v}_2$. It can be seen that outside of the diffuse interface the calculated velocities match perfectly with the analytical velocity profiles for a sharp interface. This is true regardless of the interface width (as long as $\delta \ll L$) and the viscosity ratio. Such a behavior is of great advantage in simulations of complex two-phase flows, because the velocity outside of the diffuse interface is not influenced by the velocity inside of it and the interface width can be chosen artificially large. Inside the diffuse interface the mixture and individual phase velocities vary smoothly to accommodate the changes in slope. The lower panels clearly show the presence of a slip velocity between the two phases inside the diffuse interface. The velocity of phase 1 reaches a constant value in phase 2 (i.e., as $\phi_1 \to 0$), and vice versa, that is equal to the velocity of the sharp interface, $v_\mathrm{i} = V/(r_\mu + 1)$. In this example, a viscosity ratio of 10^3 already results in the velocity of phase 1 to be essentially zero (i.e., $\bar{v}_1/V \leq 1/1001$), which illustrates that in Case I a solid can be modeled as a fluid with a large viscosity.

The above results are based on assuming that the value of the dimensionless constant h for a system where the velocity is non-zero in both phases is the same as the one determined in Ref. [3] for a solid–liquid system with flow in only the liquid (i.e., 2.757). Fig. 8 shows calculated mixture velocity profiles for three different choices of h: 0.02757, 2.757, and 275.7. It can be seen that the profiles outside of the diffuse interface for $h = 0.02757$ and 275.7 do not match the solution for a sharp interface, and the results would be highly interface width dependent. On the other hand, $h = 2.757$ provides the good match already noted in Fig. 7, regardless of the interface width and viscosity ratio. Hence, $h = 2.757$ is the correct value in a general situation involving flow in both phases (Case I). Recall that the exact value of 2.757 was determined in Ref. [3] using a matched asymptotic analysis.

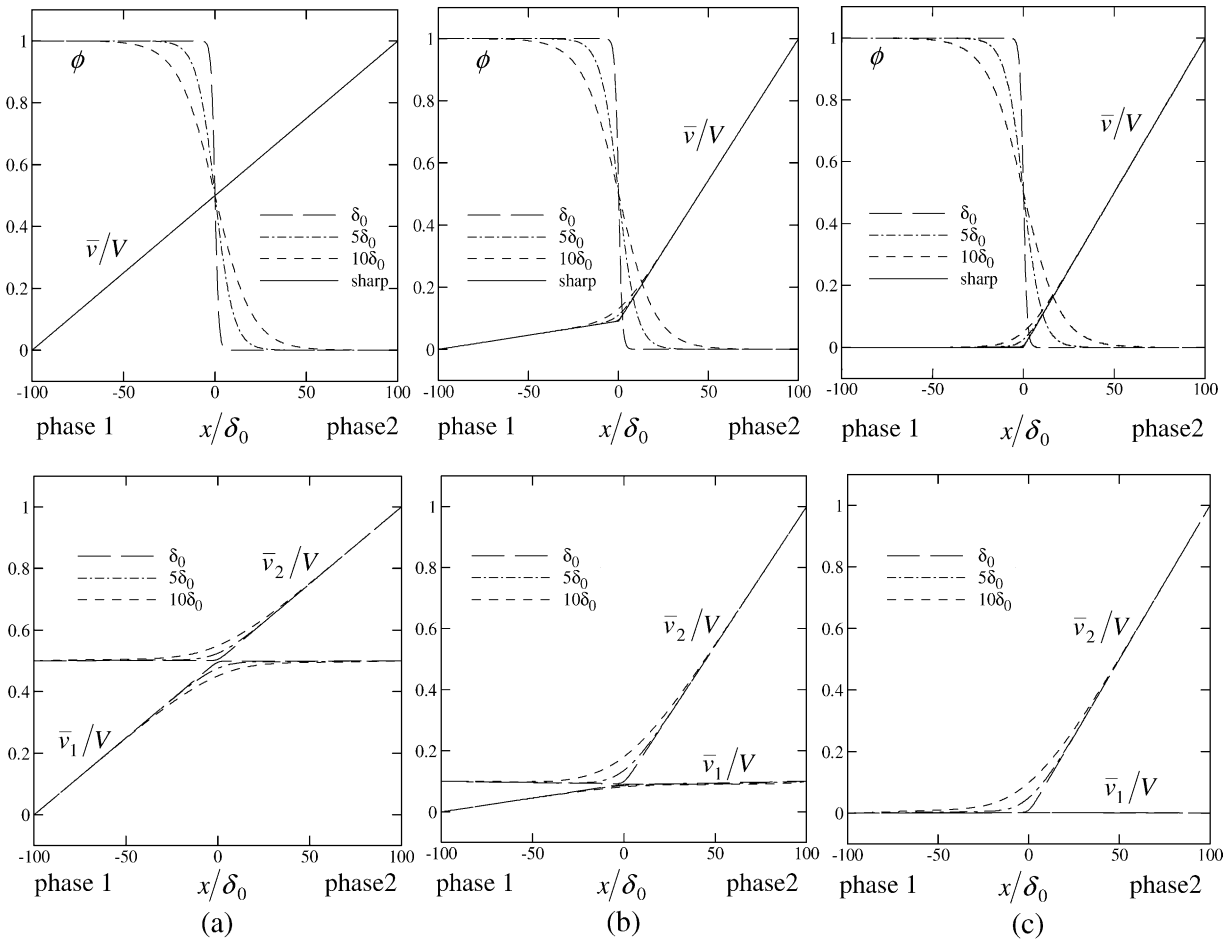

Fig. 7. Calculated velocity profiles for Case I for the two-phase shear flow system illustrated in Fig. 6 as a function of the diffuse interface width ($\delta = \delta_0$, $5\delta_0$, and $10\delta_0$): (a) $r_\mu = 1$, (b) $r_\mu = 10$, and (c) $r_\mu = 10^3$. The upper panels show the phase-field and mixture velocity profiles and the lower panels show the individual phase velocity profiles.

8.1.2. Case II

For Case II ($\bar{v}_1 = 0$), the momentum equation for phase 2 reduces to

$$0 = \frac{\mathrm{d}^2}{\mathrm{d}x^2}[(1-\phi)\bar{v}_2] - \frac{\phi h S}{\delta}\bar{v}_2. \tag{49}$$

Fig. 9 shows the calculated velocity profile in terms of the superficial velocity, $(1-\phi)\bar{v}_2$, as well as the corresponding sharp interface solution, for three different interface widths. The results are very similar to the ones for Case I with $r_\mu = 10^3$ in Fig. 7c, and show again that the velocity profile outside the diffuse interface is not influenced by the interface width. Since Eq. (49) is much easier to solve than the coupled Eqs. (47) and (48), it is clear that if one of the phases is rigid and stationary, the approach taken in Case II is of great advantage. Furthermore, no artificial viscosity needs to be assigned to the rigid phase.

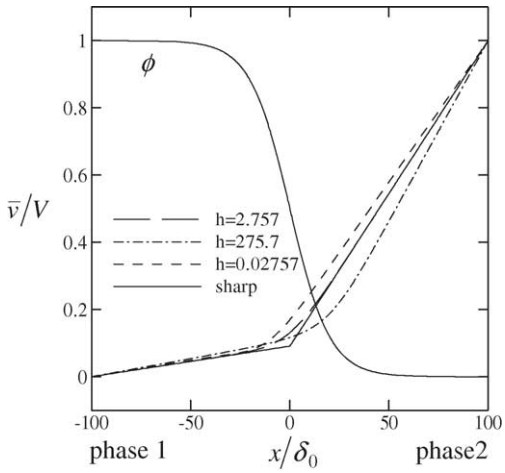

Fig. 8. Calculated velocity profiles for Case I for the two-phase shear flow system illustrated in Fig. 6 for $h = 2.757$, 275.7, and 0.02757 ($\delta = 10\delta_0$ and $r_\mu = 10$).

8.1.3. Case III

The momentum equation for Case III ($\bar{v}_1 = \bar{v}_2 = \bar{v}$) reduces for this example to

$$0 = \frac{\mathrm{d}}{\mathrm{d}x}\left(\bar{\mu}\frac{\mathrm{d}\bar{v}}{\mathrm{d}x}\right) \tag{50}$$

where $\bar{\mu} = \phi\mu_1 + (1-\phi)\mu_2$ is the mixture viscosity, as before. Fig. 10a–c shows the calculated velocity profiles for viscosity ratios, r_μ, of 1, 10, and 10^3, respectively, and three different interface widths. The results are compared with the corresponding sharp interface solution. It can be seen that other than for $r_\mu = 1$, the velocities are highly dependent on the diffuse interface width and the slopes of the velocity profiles outside of the diffuse interface are generally not in agreement with the sharp interface solution.

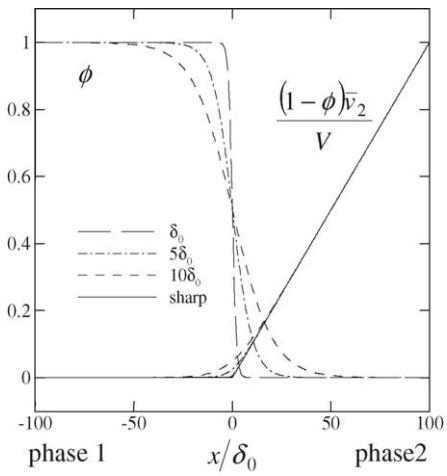

Fig. 9. Calculated velocity profiles for Case II for the two-phase shear flow system illustrated in Fig. 6 as a function of the diffuse interface width ($\delta = \delta_0$, $5\delta_0$, and $10\delta_0$).

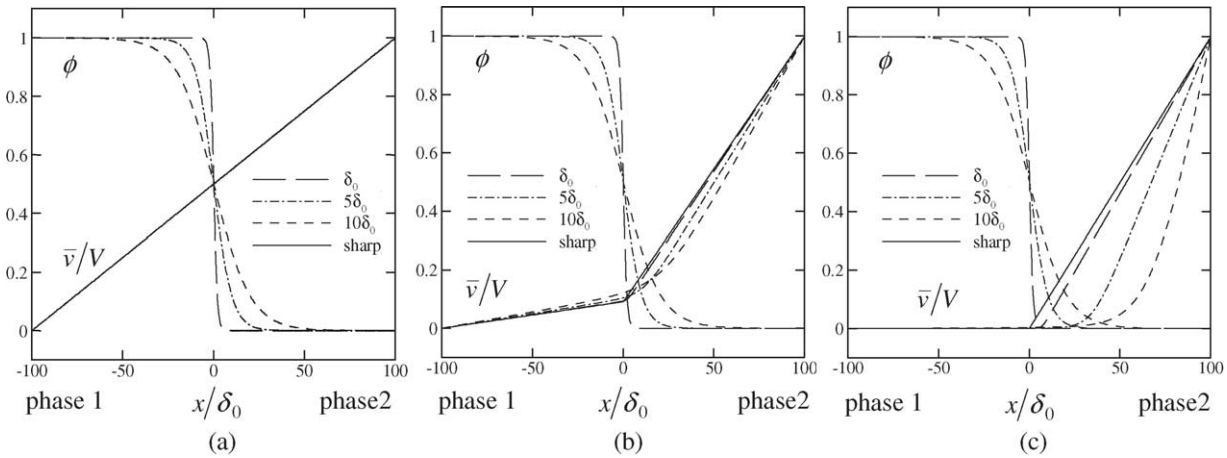

Fig. 10. Calculated velocity profiles for Case III for the two-phase shear flow system illustrated in Fig. 6 as a function of the diffuse interface width ($\delta = \delta_0$, $5\delta_0$, and $10\delta_0$): (a) $r_\mu = 1$, (b) $r_\mu = 10$, and (c) $r_\mu = 10^3$.

Hence, in actual computations of two-phase flows that involve a large viscosity ratio, the interface width has to be chosen extremely small in order to approach the sharp interface solution. In fact, since Case III is equivalent to thermodynamically derived models [12], δ should be chosen equal to the physical width of a diffuse interface, which is of atomic scale. This example clearly illustrates the advantage of a full two-phase approach where a velocity slip is allowed inside the diffuse interface (Cases I and II), as opposed to assuming that both phases have a single velocity (Case III). While a different function for the mixture viscosity might produce better agreement [31], it is unclear how such a function could be chosen in a physically meaningful way.

8.2. Normal flow due to phase-change in the presence of a density difference

The second example is illustrated in Fig. 11 and considers a one-dimensional flow normal to a planar diffuse interface that is induced by phase-change in the presence of a density difference between the phases. The densities and viscosities, ρ_k and μ_k, are assumed constant but differ between the phases. The interface moves at a constant speed V_i into the positive x-direction. The problem becomes steady if one introduces the moving coordinate $x = x' - V_i t$, where x' is the fixed coordinate normal to the interface. The far-field velocity of phase 1 ($x \to -\infty$) is taken to be zero, and the far-field pressure in phase 2, $\bar{p}_{2,\infty}$, is used as a known reference pressure.

In this example, the velocities are solely determined by mass conservation and are the same in Cases I, II, and III. In the moving coordinate system, the mixture continuity equation, Eq. (16), which is valid even for unequal

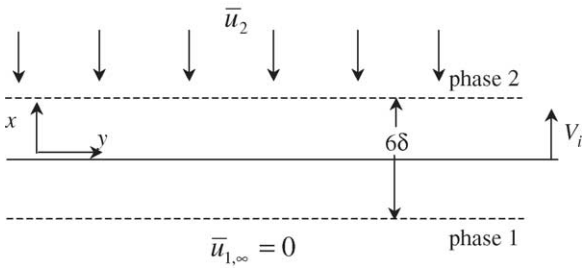

Fig. 11. Schematic illustration of the system used in the analysis of normal flow due to phase-change in the presence of a density difference between the phases.

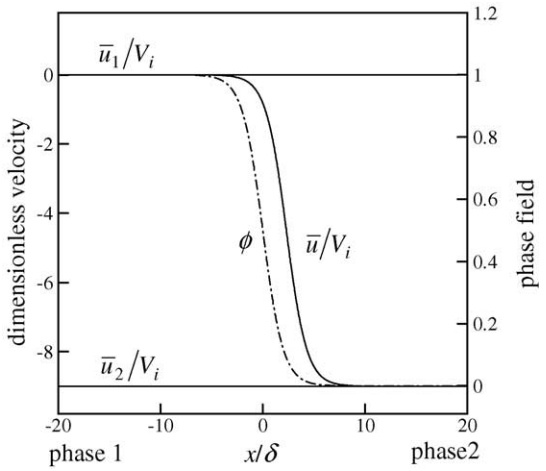

Fig. 12. Velocity profiles for one-dimensional flow normal to a diffuse interface due to phase-change with a density ratio of $r_\rho = 10$.

phase velocities, becomes

$$\frac{\mathrm{d}}{\mathrm{d}x}[\bar{\rho}(\bar{u} - V_\mathrm{i})] = 0 \tag{51}$$

which can be integrated to yield

$$\bar{u} = -V_\mathrm{i}\left(\frac{\rho_1}{\bar{\rho}} - 1\right). \tag{52}$$

The continuity equations for each phase, Eq. (14), become

$$\frac{\mathrm{d}}{\mathrm{d}x}[\rho_1\phi_1(\bar{u}_1 - V_\mathrm{i})] = \Gamma_1 \tag{53}$$

$$\frac{\mathrm{d}}{\mathrm{d}x}[\rho_2\phi_2(\bar{u}_2 - V_\mathrm{i})] = \Gamma_2. \tag{54}$$

For constant ρ_1 and ρ_2, and using the definition for Γ_1 and Eq. (15), Eqs. (53) and (54) can be integrated to yield

$$\bar{u}_1 = 0 \quad \text{and} \quad \bar{u}_2 = -V_\mathrm{i}\left(\frac{\rho_1}{\rho_2} - 1\right). \tag{55}$$

Hence, the individual phase velocities are constant. It can be easily verified that Eq. (55) and the definition of the mixture velocity, $\bar{u} = (\rho_1\phi_1\bar{u}_1 + \rho_2\phi_2\bar{u}_2)/(\rho_1\phi_1 + \rho_2\phi_2)$, lead to Eq. (52). It can also be shown that the interfacial velocities due to phase change are given by $\bar{u}_{1,\Gamma} = \bar{u}_1$ and $\bar{u}_{2,\Gamma} = \bar{u}_2$. Fig. 12 shows the variation of the velocities across the diffuse interface for a density ratio $r_\rho = \rho_1/\rho_2$ of 10. Note that the mixture velocity profile is not symmetric with respect to $\phi = 0.5$.

8.2.1. Case I

For Case I, the x-momentum equations for each phase reduce to

$$\phi\frac{\mathrm{d}\bar{p}_1}{\mathrm{d}x} = -\frac{4}{3}\frac{\mathrm{d}}{\mathrm{d}x}\left[\frac{\mathrm{d}\phi}{\mathrm{d}x}\frac{\mu_1\mu_2\phi}{\mu_1(1-\phi)+\phi\mu_2}\bar{u}_2\right] + \frac{\mu_1\mu_2}{\mu_1(1-\phi)+\phi\mu_2}\frac{\phi(1-\phi)hS}{\delta}\bar{u}_2 - \sigma\phi(1-\phi)\frac{\mathrm{d}}{\mathrm{d}x}\left(\frac{\mathrm{d}S}{\mathrm{d}\phi}\right) \tag{56}$$

$$(1-\phi)\frac{\mathrm{d}\bar{p}_2}{\mathrm{d}x} = -\frac{4}{3}\frac{\mathrm{d}}{\mathrm{d}x}\left[\frac{\mathrm{d}\phi}{\mathrm{d}x}\frac{\mu_1\mu_2(1-\phi)}{\mu_1(1-\phi)+\phi\mu_2}\bar{u}_2\right] - \frac{\mu_1\mu_2}{\mu_1(1-\phi)+\phi\mu_2}\frac{\phi(1-\phi)hS}{\delta}\bar{u}_2 + \sigma\phi(1-\phi)\frac{\mathrm{d}}{\mathrm{d}x}\left(\frac{\mathrm{d}S}{\mathrm{d}\phi}\right) \tag{57}$$

Since the velocity $\bar{u}_2$ is known, Eqs. (56) and (57) are easily integrated to obtain the variation of the phase pressures across the diffuse interface. Calculations are performed for an interfacial Reynolds number, $Re = \rho_2 V_\mathrm{i}\delta/\mu_2$, of 10^{-3} and an interfacial Weber number, $We = \rho_2 V_\mathrm{i}^2\delta/\sigma$, of 10^{-5}. These two parameters arise from non-dimensionalizing Eqs. (56) and (57). Fig. 15 shows the computed profiles of the dimensionless mixture pressure, defined as $p^* = (\bar{p} - \bar{p}_{2,\infty})/(\sigma/\delta)$, together with the phase-field in the upper panels, and of the dimensionless pressures of each phase, defined as $p_1^* = (\bar{p}_1 - \bar{p}_{2,\infty})/(\sigma/\delta)$ and $p_2^* = (\bar{p}_2 - \bar{p}_{2,\infty})/(\sigma/\delta)$, in the lower panels. Pressure profiles are provided for density ratios, r_ρ, of 1, 30, and 100 with a viscosity ratio of $r_\mu = 1$ in Fig. 13a, and for $r_\mu = 1$, 30, and 100 with $r_\rho = 100$ in Fig. 13b.

Applying the interfacial momentum jump condition, i.e., the second of Eq. (18), to the present example, the difference between the far-field pressures on either side of the interface is given by

$$\bar{p}_{1,\infty} - \bar{p}_{2,\infty} = V_\mathrm{i}^2\rho_1\left(\frac{\rho_1}{\rho_2} - 1\right). \tag{58}$$

This pressure difference is often referred to as the "vapor recoil" effect in a liquid–vapor system. It can be verified from Fig. 13 that the calculated pressures in Case I follow Eq. (58). Increasing r_ρ results in a larger far-field pressure difference, whereas increasing r_μ has no effect on this difference. The pressure profiles for $r_\rho = 1$ (i.e., no flow) in Fig. 13a are the same as those in Figs. 5a and B1a, and the mixture pressure p^* shows the hump inside the diffuse interface that is a manifestation of the capillary stress. Increasing r_ρ (Fig. 13a) or r_μ (Fig. 13b) both increases the magnitude of the hump, indicating that in the presence of a normal flow a hump would be present even in the absence of surface tension. Note that the pressures of each phase, p_k^* (lower panels in Fig. 13), reach well-defined values as the phase fraction ϕ_k vanishes. The difference between the phase pressures at a given location changes with both r_ρ and r_μ.

8.2.2. Case II

In Case II, the momentum equation for phase 2 reduces to

$$(1-\phi)\frac{\mathrm{d}\bar{p}_2}{\mathrm{d}x} = \mu_2\frac{4}{3}\frac{\mathrm{d}^2}{\mathrm{d}x^2}[(1-\phi)\bar{u}_2] - \frac{\mu_2\phi hS}{\delta}\bar{u}_2 + \sigma\phi(1-\phi)\frac{\mathrm{d}}{\mathrm{d}x}\left(\frac{\mathrm{d}S}{\mathrm{d}\phi}\right). \tag{59}$$

Note that Eq. (59) can be obtained from Eq. (57) of Case I in the limit of $\mu_1 \to \infty$, since $\bar{u}_1 = 0$ in both cases for this example. With $\bar{u}_2$ known, Eq. (59) is easily integrated to obtain the $\bar{p}_2$ profile across the diffuse interface. Results in terms of the dimensionless pressure p_2^* (defined as in Case I) are shown in Fig. 14 for three different density ratios. For $r_\rho = 1$, i.e., in the absence of flow, the variation of p_2^* is identical to the one shown in Fig. B1a. In the presence of flow ($r_\rho = 30$ and 100), p_2^* decreases almost linearly as $\phi_2 = 1 - \phi$ approaches zero. This linear decrease indicates that the interfacial drag term, i.e., the second term on the right-hand side of Eq. (59), becomes dominant as $\phi_2 \to 0$. Since the drag is linearly proportional to the velocity, and $\bar{u}_2$ is constant in the present example, the pressure gradient is constant and p_2^* decreases linearly. Physically, p_2^* has little meaning as $\phi_2 \to 0$ (i.e., inside phase 1) and Eq. (59) becomes trivial. To avoid numerical difficulties when solving Eq. (59) with p_2^* approaching infinitely small values as $\phi_2 \to 0$, a small "cutoff" value (say 10^{-6}) should be used for ϕ_2.

8.2.3. Case III

The mixture momentum equation for Case III can be expressed in the moving coordinate system as:

$$\frac{\mathrm{d}}{\mathrm{d}x}[\bar{\rho}(\bar{u} - V_\mathrm{i})\bar{u}] = -\frac{\mathrm{d}\bar{p}}{\mathrm{d}x} + \frac{4}{3}\frac{\mathrm{d}}{\mathrm{d}x}\left(\bar{\mu}\frac{\mathrm{d}\bar{u}}{\mathrm{d}x}\right) - \sigma\frac{\mathrm{d}S}{\mathrm{d}\phi}\frac{\mathrm{d}\phi}{\mathrm{d}x}. \tag{60}$$

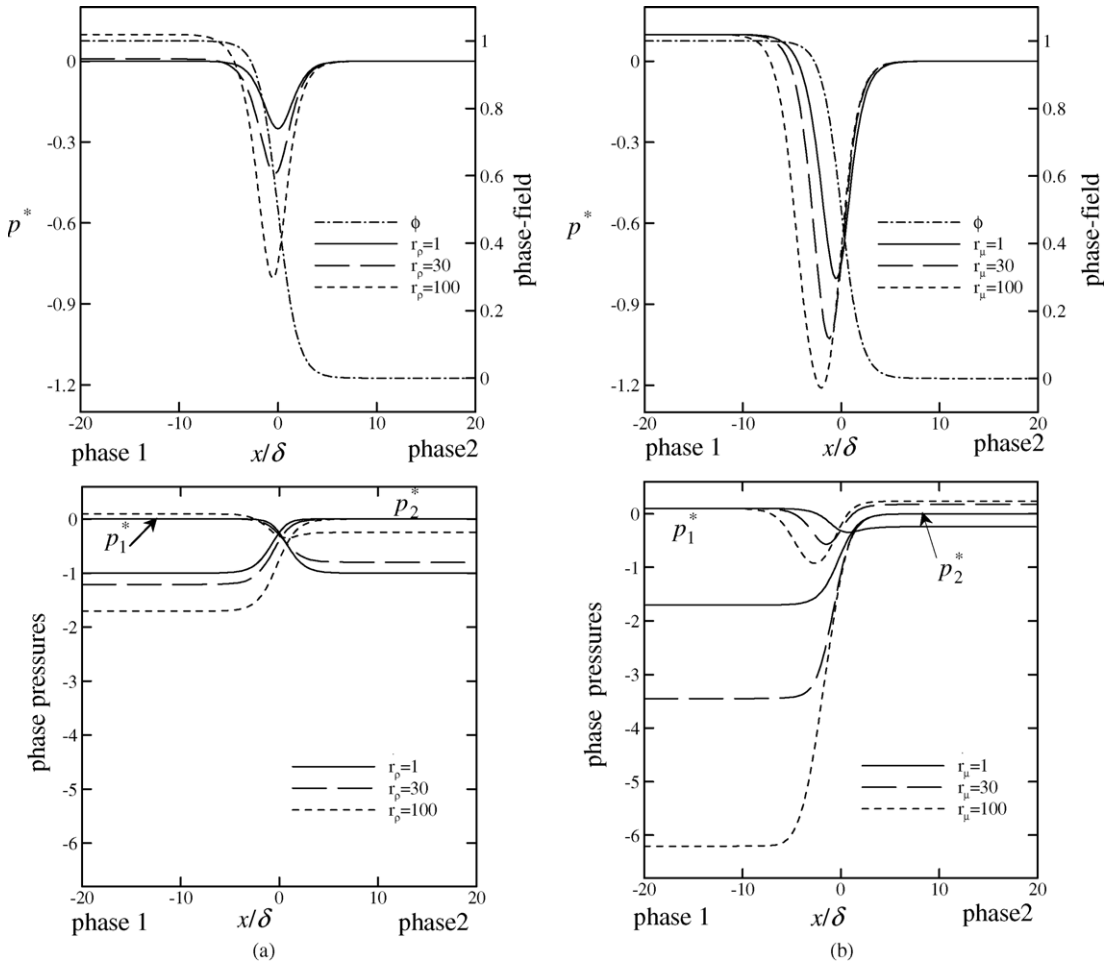

Fig. 13. Calculated pressure profiles for Case I for flow normal to a diffuse interface as illustrated in Fig. 11: (a) $r_\rho = 1$, 30, and 100 and $r_\mu = 1$, and (b) $r_\mu = 1$, 30, and 100 and $r_\rho = 100$ ($Re = 10^{-3}$ and $We = 10^{-5}$).

Substituting Eq. (52) for the mixture velocity and integrating yields the following analytical solution for the mixture pressure variation

$$\bar{p} - \bar{p}_{2,\infty} = V_i^2 \rho_1 \left(\frac{\rho_1}{\rho_2} - \frac{\rho_1}{\bar{\rho}} \right) + \frac{4}{3} \bar{\mu} V_i \frac{\rho_1}{\bar{\rho}^2} (\rho_1 - \rho_2) \frac{\mathrm{d}\phi}{\mathrm{d}x} - \frac{\sigma}{\delta} \phi (1 - \phi). \tag{61}$$

It can be seen that Eq. (61), when evaluated at $\phi = 1$, reduces to Eq. (58) for the "vapor recoil" pressure difference, since the last two terms in Eq. (61) vanish in the bulk phases. Rewriting Eq. (61) in terms of the dimensionless mixture pressure $p^* = (\bar{p} - \bar{p}_{2,\infty})/(\sigma/\delta)$ reveals that p^* is a function of r_ρ, r_μ, Re, and We, as in Case I.

Fig. 15 shows the calculated mixture pressure profiles for the same parameter ranges as in Fig. 13 for Case I. Hence, Fig. 15 can be compared directly to the upper panels of Fig. 13. Although the two models corresponding to Cases I and III give the same results for the far-field pressure difference, the mixture pressures inside the diffuse interface vary in a somewhat different fashion. With increasing r_ρ the mixture pressure profile in Case III (Fig. 15a) develops a "double hump", and the depths of the humps do not vary appreciably with r_ρ. The "double hump"

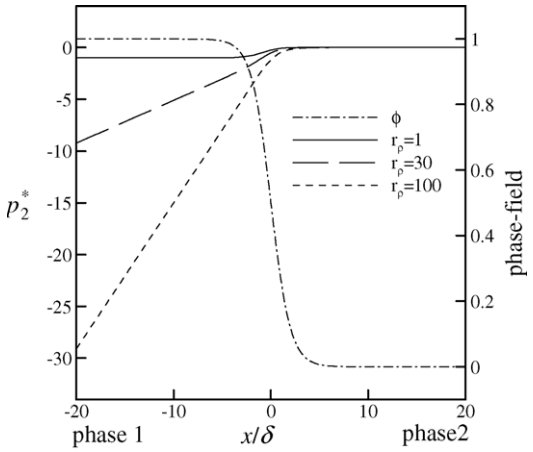

Fig. 14. Calculated pressure profiles for Case II for flow normal to a diffuse interface as illustrated in Fig. 11: $r_\rho = 1$, 30, and 100 ($Re = 10^{-3}$ and $We = 10^{-5}$).

disappears again with increasing r_μ (Fig. 15b). The appearance of the "double hump" in Case III can be attributed to the asymmetric nature of the mixture velocity profile across the diffuse interface, as shown in Fig. 12. Recall that Case III is equivalent to the thermodynamically derived model in Ref. [12], and other choices for the mixture density and viscosity variations, $\overline{\rho}$ and $\overline{\mu}$, inside the diffuse interface would result in different mixture pressure profiles. Hence, the physical significance of the "double humps" in Fig. 15 is not entirely clear. Also note that for increasing r_ρ, the mixture pressure profile in Case III extends increasingly into phase 2 (Fig. 15a), which again can be attributed to the asymmetric nature of the mixture velocity profile. In fact for $r_\rho = 100$, the minimum in the second hump occurs at approximately $\phi = 0.01$, which can be regarded as being outside of the diffuse interface. In contrast, for Case I the width of the mixture pressure hump does not change with r_ρ and the hump is well confined within the diffuse interface (Fig. 13a). As with the velocity profile in the first example (Section 8.1.3), the strong

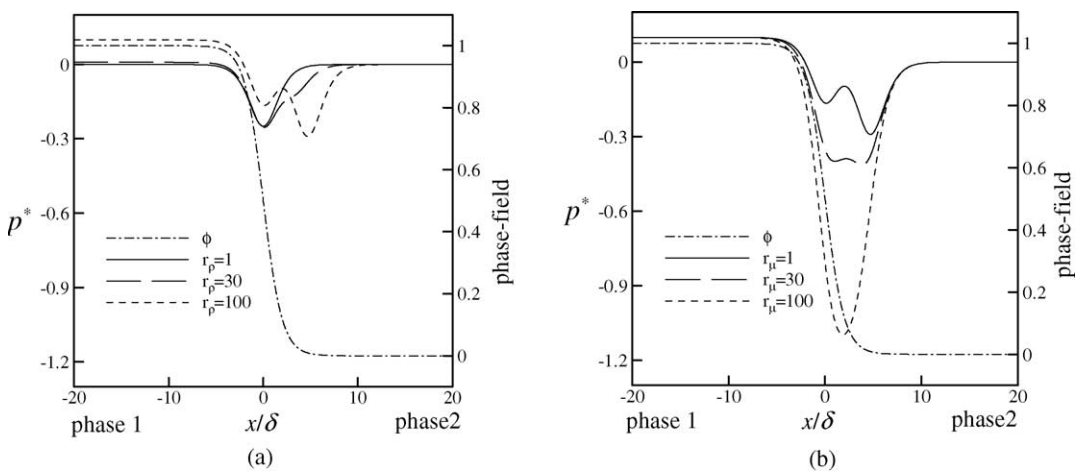

Fig. 15. Calculated pressure profiles for Case III for flow normal to a diffuse interface as illustrated in Fig. 11: (a) $r_\rho = 1$, 30, and 100 and $r_\mu = 1$, and (b) $r_\mu = 1$, 30, and 100 and $r_\rho = 100$ ($Re = 10^{-3}$ and $We = 10^{-5}$).

dependence of the pressure profile on the interface width and on the mixture property variations, $\overline{\rho}$ and $\overline{\mu}$, creates a large ambiguity in Case III.

9. Conclusions

A diffuse interface model for two-phase flows with phase-change and surface tension is derived using an ensemble averaging approach. The derivations start from well-established local sharp interface balances and the diffuse interface is viewed as a superposition of microscopic (atomic-scale) and macroscopic (averaged) morphologies. The present model assumes that the two phases coexist inside the diffuse interface and have different velocities and pressures. Interactions between the phases and interfacial sources, including the capillary stress, are modeled explicitly.

The present model is tested for two simple one-dimensional two-phase flows. In each case, the results are compared to those from a simplified mixture version, where the velocities of the phases inside the diffuse interface are assumed equal, that is equivalent to a thermodynamically derived model [12]. Furthermore, the special case of one phase being rigid and stationary is examined by either letting its viscosity approach infinity [12] or setting its velocity to zero and not solving any equations for that phase [3]. It is shown that the present two-phase approach gives results that are generally independent of the diffuse interface width, such that the variation of the velocity and pressure outside of the diffuse interface does not depend on the variation of the variables inside of it. This property is of great advantage in large-scale simulations of two-phase flows [3], because it allows computations to be performed for arbitrarily large diffuse interface widths (as long as the width is smaller than the average radius of curvature to be resolved). The mixture approach, although somewhat simpler and also equivalent to thermodynamically derived models, does not possess this property. In both approaches, however, the depth of the pressure hump that is induced by the capillary stress is inversely proportional to the diffuse interface width. Hence, in order to resolve flows at the scale of the diffuse interface, e.g., breakup or merging of interfaces, its width must be chosen in a physically realistic way, as expected.

To complete the theory for two-phase flows, an evolution equation for the phase-field variable ϕ is needed for non-equilibrium situations. Such a phase-field equation is derived in Ref. [3], using the same two-phase averaging approach, for the case of solidification. A generalization to the kind of two-phase flows considered here will be presented in a forthcoming publication [28].

Acknowledgement

This work was supported by the U.S. National Science Foundation under Grant No. DMR-0132225.

Appendix A. Limiting cases for the average shear stress

The general expression for the average shear stress given by Eq. (35) is examined further by applying it to the limiting cases discussed in Section 2 and illustrated in Fig. 1. In the limit of Case II, applying Eq. (35) to the fluid, phase 2, only and setting $\overline{\boldsymbol{u}}_1 = 0$ yields

$$\phi_2\overline{\boldsymbol{\tau}}_2 = \mu_2\left[\nabla(\phi_2\overline{\boldsymbol{u}}_2) + \nabla(\phi_2\overline{\boldsymbol{u}}_2)^{\mathrm{T}} - \frac{2}{3}\nabla\cdot(\phi_2\overline{\boldsymbol{u}}_2)\boldsymbol{I}\right], \quad \text{for Case II.} \tag{A.1}$$

Eq. (A.1) is identical to the expression usually employed in flow through porous media [24], where the average viscous stress is taken to be proportional to the gradient of the superficial velocity, $\phi_2\overline{\boldsymbol{u}}_2$. Substituting the continuity equation, assuming constant density and viscosity, and taking the divergence of Eq. (A.1) results in $\nabla\cdot(\phi_2\overline{\boldsymbol{\tau}}_2) = \mu_2(\nabla^2(\phi_2\overline{\boldsymbol{u}}_2) + 1/3\nabla[\Gamma_2(1/\rho_2 - 1/\rho_1)])$ for Case II. This illustrates that the average viscous stress contains a contribution due to flows that arise in the presence of phase-change and a density difference between the phases.

Applying Eq. (35) to Case III ($\bar{\boldsymbol{u}}_1 = \bar{\boldsymbol{u}}_2 = \bar{\boldsymbol{u}}$), the average viscous stress of the mixture is given by:

$$\bar{\boldsymbol{\tau}} = \phi_1 \bar{\boldsymbol{\tau}}_1 + \phi_2 \bar{\boldsymbol{\tau}}_2 = \bar{\mu}\left(\nabla \bar{\boldsymbol{u}} + \nabla \bar{\boldsymbol{u}}^{\mathrm{T}} - \frac{2}{3}(\nabla \cdot \bar{\boldsymbol{u}})\boldsymbol{I}\right), \quad \text{for Case III} \tag{A.2}$$

where $\bar{\mu} = \phi_1\mu_1 + \phi_2\mu_2$. The term $-2/3(\nabla \cdot \bar{\boldsymbol{u}})\boldsymbol{I}$ accounts for the compressibility of the mixture inside the diffuse interface for $\rho_1 \neq \rho_2$ (see Eq. (16)). Eq. (A.2) is identical to the constitutive relation for the viscous stress used in the thermodynamically derived model of Anderson et al. [12]. Although the expression $\bar{\mu} = \phi_1\mu_1 + \phi_2\mu_2$ for the mixture viscosity arises naturally in the present derivations, it should be kept in mind that μ_1 and μ_2 are actually effective viscosities (see Eq. (31)) that could depend on the phase fractions ϕ_k. If one chooses a more complex model for the effective viscosities, a different relation for $\bar{\mu}$ would result.

Returning to Case I ($\bar{\boldsymbol{u}}_1 \neq \bar{\boldsymbol{u}}_2$), but considering the limit where phase 1 is a solid that is modeled as a fluid with a large viscosity, i.e. $\mu_1 \gg \mu_2$, Eq. (35) for phase 1 reduces to

$$\phi_1 \bar{\boldsymbol{\tau}}_1 = \mu_1\phi_1\left(\nabla \bar{\boldsymbol{u}}_1 + \nabla \bar{\boldsymbol{u}}_1^{\mathrm{T}} - \frac{2}{3}(\nabla \cdot \bar{\boldsymbol{u}}_1)\boldsymbol{I}\right), \quad \text{for Case I with } \mu_1 \gg \mu_2. \tag{A.3}$$

Then, with μ_1 very large and $\bar{\boldsymbol{\tau}}_1$ finite, Eq. (A.3) indicates that in this limit the gradients of $\bar{\boldsymbol{u}}_1$ will vanish and phase 1 will be like a rigid body. This would not be the case if $\bar{\boldsymbol{\tau}}_1$ were proportional to the gradient of the superficial velocity, $\phi_1\bar{\boldsymbol{u}}_1$, in this limit, because ϕ_1 varies inside the diffuse interface. For $\mu_1 \gg \mu_2$ Eq. (35) for phase 2 reduces to Eq. (A.1), which was originally obtained by assuming $\bar{\boldsymbol{u}}_1 = 0$.

Appendix B. Variation of the pressures across the diffuse interface due to surface tension

The expression for the interfacial force density due to curvature variations in the presence of surface tension given by Eq. (40) is examined in this appendix for macroscopically planar and spherical interfaces in the absence of flow and gravity. Under these assumptions, the variation of the pressures of the two phases, $\bar{p}_1$ and $\bar{p}_2$, across the diffuse interface can be obtained from $\phi_1\nabla\bar{p}_1 = \boldsymbol{M}_1^{\sigma}$ and $\phi_2\nabla\bar{p}_2 = \boldsymbol{M}_2^{\sigma}$, respectively. Results are shown in Fig. B1 for the choice $a = b = 1$ and $S_0 = 1/\delta$ in Eq. (8). The dimensionless phase pressures plotted in Fig. B1 are defined as $p_1^* = (\bar{p}_1 - \bar{p}_{2,\infty})/(\sigma/\delta)$ and $p_2^* = (\bar{p}_2 - \bar{p}_{2,\infty})/(\sigma/\delta)$, where $\bar{p}_{2,\infty}$ is again a reference pressure far from the interface in phase 2. The non-dimensional mixture pressure variations shown in Fig. B1a and b are identical to those

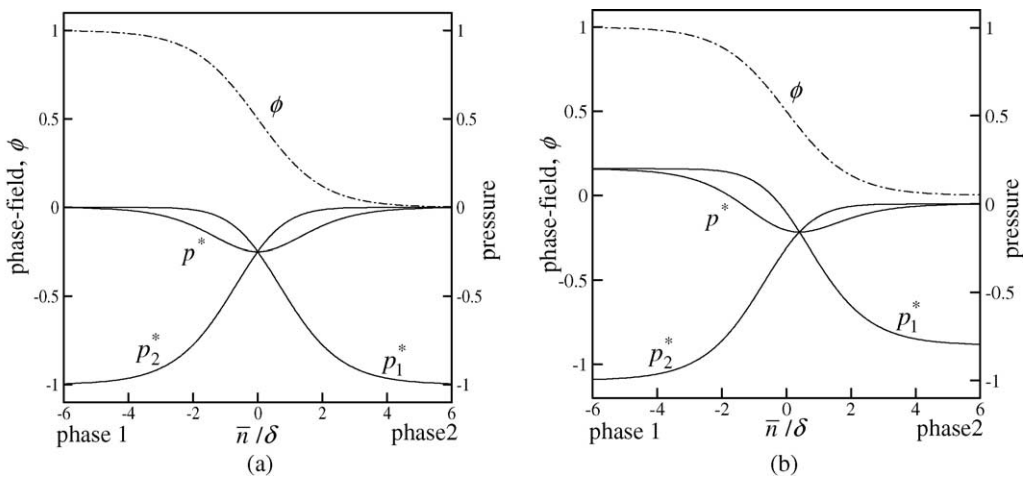

Fig. B1. Phase and mixture pressure variations inside (a) planar and (b) spherical (with $R/\delta = 10$) interfaces in equilibrium.

in Fig. 5a and b, respectively. The difference between the pressures of each phase, $\overline{p}_1 - \overline{p}_2$, at the same location is due to the combined effects of the average curvature, $\overline{\kappa}$, and the microscopic curvature of the atomic structures inside the diffuse interface, $\mathrm{d}S/\mathrm{d}\phi$, according to $\overline{p}_1 - \overline{p}_2 = \sigma(\overline{\kappa} - \mathrm{d}S/\mathrm{d}\phi)$. For a planar diffuse interface ($\overline{\kappa} = 0$; Fig. B1a), the difference between the pressures of each phase is solely due to microscopic curvatures and varies according to $\overline{p}_1 - \overline{p}_2 = -\sigma\,\mathrm{d}S/\mathrm{d}\phi = -\sigma/\delta(1 - 2\phi)$. In order to maintain this difference, the pressure of one phase must increase and the pressure of the other phase must decrease across the interface, while the mixture pressure, $\overline{p} = \phi_1\overline{p}_1 + \phi_2\overline{p}_2$, varies as already explained in connection with Fig. 5. At $\phi = 0.5$ the difference between the phase pressures vanishes because the microscopic curvature changes its sign (i.e., it is locally planar) as explained in Section 3. At $\phi = 0$ and $\phi = 1$ the pressure difference between the phases for a planar interface is equal to $\overline{p}_1 - \overline{p}_2 = \mp\sigma/\delta$, which is a physically meaningful and well-defined value. For a spherical diffuse interface, Fig. B1b, the phase pressures vary in a similar manner except that the pressure difference is given by $\overline{p}_1 - \overline{p}_2 = \sigma[2/R - (1 - 2\phi)/\delta]$.

Appendix C. Variation of the pressures across the diffuse interface due to interfacial drag

The interfacial drag model given by Eq. (43) can be better understood by considering a simple one-dimensional flow across a diffuse interface (in the $\overline{\boldsymbol{n}}$ direction) where the relative velocity, $\overline{u}_k - \overline{u}_j = (\overline{\boldsymbol{u}}_k - \overline{\boldsymbol{u}}_j)\cdot\overline{\boldsymbol{n}}$, is assumed constant and the inertia, viscous shear stress, and gravitational terms are all neglected. Then, the momentum equation for phase k reduces to

$$\phi_k \frac{\mathrm{d}\overline{p}_k}{\mathrm{d}\overline{n}} = -\frac{\mu_k\mu_j}{\mu_k\phi_j + \phi_k\mu_j}\frac{\phi_k\phi_j h S}{\delta}(\overline{u}_k - \overline{u}_j). \tag{C.1}$$

Using Eq. (8) for S with $a = b = 1$ and $S_0 = 1/\delta$, the above equation can be integrated to obtain the following expression for the variation of the dimensionless pressure of phase 1, p_1^* (redefined from Fig. B1), across the diffuse interface

$$p_1^* = \frac{\overline{p}_1 - \overline{p}_{1,\infty}}{(\mu_1/\delta)(\overline{u}_1 - \overline{u}_2)} = -\int \frac{\phi_1\phi_2^2 h}{\phi_1 + \phi_2 r_\mu}\,\mathrm{d}\left(\frac{\overline{n}}{\delta}\right) \tag{C.2}$$

where the viscosity ratio is defined as $r_\mu = \mu_1/\mu_2$. This pressure is plotted in Fig. C1 for viscosity ratios of 1, 10, and 1000. Because of the drag between the two phases, the pressure of phase 1 decreases in the direction of the flow from

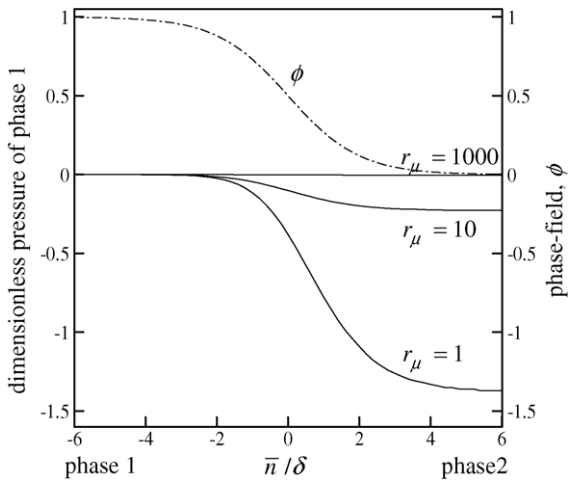

Fig. C1. Variation of the dimensionless pressure of phase 1 given by Eq. (C.2) across the diffuse interface for viscosity ratios of 1, 10, and 1000.

phase 1 towards phase 2 (i.e., $(\bar{u}_1 - \bar{u}_2) > 0$). The majority of the pressure drop occurs for $\phi = \phi_1 < 0.5$. This can be explained by the fact that the drag experienced by phase 1 increases with increasing volume fraction of phase 2. If one views the diffuse interface as a porous medium in the limit of $\bar{u}_2 = 0$, the increasing drag can be visualized as being caused by the permeability decreasing with increasing volume fraction of the porous matrix (phase 2). More generally, Eq. (C.1) can be thought of as a modified Darcy's law (in 1D) for the relative flow of two viscous fluids. Such a law could find use in numerous applications other than diffuse interface modeling. Fig. C1 also indicates that the total pressure drop across the diffuse interface decreases with increasing viscosity ratio. Since the pressure is non-dimensionalized with μ_1, increasing the viscosity ratio should be viewed as decreasing μ_2 while keeping μ_1 constant. The pressure drop in phase 1 decreases with decreasing μ_2 because the "matrix" (i.e., phase 2) deforms more easily. In the limit of $r_\mu \to \infty$, phase 2 can offer no resistance to the flow and the pressure drop in phase 1 vanishes.

References

[1] D.M. Anderson, G.B. McFadden, A.A. Wheeler, Diffuse-interface methods in fluid mechanics, Annu. Rev. Fluid Mech. 30 (1998) 139–165.
[2] J.U. Brackbill, D.B. Kothe, C.A. Zemach, A continuum method for modeling surface tension, J. Comput. Phys. 100 (1992) 335–354.
[3] C. Beckermann, H.-J. Diepers, I. Steinbach, A. Karma, X. Tong, Modeling melt convection in phase-field simulations of solidification, J. Comput. Phys. 154 (1999) 468–496.
[4] R. Scardovelli, S. Zaleski, Direct numerical simulation of free-surface and interfacial flow, Annu. Rev. Fluid Mech. 31 (1999) 567–603.
[5] S. Osher, R.P. Fedkiw, Level set methods: an overview and some recent results, J. Comput. Phys. 169 (2001) 463–502.
[6] S. Chen, G.D. Doolen, Lattice Boltzmann method for fluid flows, Annu. Rev. Fluid Mech. 30 (1998) 329–364.
[7] G. De Fabritiis, A. Mancini, D. Mansutti, S. Succi, Mesoscopic models of liquid/solid phase transitions, Int. J. Mod. Phys. C 9 (1998) 1405–1415.
[8] W. Miller, S. Succi, D. Mansutti, Lattice Boltzmann model for anisotropic liquid–solid phase transition, Phys. Rev. Lett. 86 (2001) 3578–3581.
[9] T. Lee, C.-L. Lin, Pressure evolution lattice-Boltzmann-equation method for two-phase flow with phase change, Phys. Rev. E 67 (2003) 056703.
[10] W.J. Boettinger, J.A. Warren, C. Beckermann, A. Karma, Phase-field simulation of solidification, Annu. Rev. Mater. Res. 32 (2002) 163–194.
[11] D. Jacqmin, Calculation of two-phase Navier–Stokes flows using phase-field modeling, J. Comput. Phys. 155 (1999) 96–127.
[12] D.M. Anderson, G.B. McFadden, A.A. Wheeler, A phase-field model of solidification with convection, Physica D 135 (2000) 175–194.
[13] M. Conti, Density change effects on crystal growth from the melt, Phys. Rev. E 64 (2001) 051601.
[14] L.K. Antanovskii, Microscale theory of surface tension, Phys. Rev. E 54 (1996) 6285–6290.
[15] H.T. Davis, L.E. Scriven, Stress and structure in fluid interfaces, Adv. Chem. Phys. 49 (1982) 357–454.
[16] D. Jamet, O. Lebaigue, N. Coutris, J.M. Delhaye, The second gradient method for the direct numerical simulation of liquid–vapor flows with phase change, J. Comput. Phys. 169 (2001) 624–651.
[17] D.M. Anderson, G.B. McFadden, A.A. Wheeler, A phase-field model with convection: sharp-interface asymptotics, Physica D 151 (2001) 305–331.
[18] D.A. Drew, Mathematical modeling of two-phase flow, Annu. Rev. Fluid Mech. 15 (1983) 261–291.
[19] D.A. Drew, S.L. Passman, Theory of Multicomponent Fluids, Applied Mathematical Sciences 135, Springer-Verlag, New York, 1999.
[20] D. Bercovici, Y. Ricard, G. Schubert, A two-phase model for compaction and damage: 1. General theory, J. Geophys. Res. 106 (2001) 8887–8906.
[21] M. Ishii, Thermo-Fluid Dynamic Theory of Two-Phase Flow, Eyrolles, Paris, 1975.
[22] C. Kleinstreuer, Two-Phase Flow: Theory and Applications, Taylor & Francis, New York, 2003.
[23] J. Ni, C. Beckermann, A volume-averaged two-phase model for transport phenomena during solidification, Metall. Trans. B 22B (1991) 349–361.
[24] M. Kaviany, Principles of Convective Heat Transfer, second ed., Springer-Verlag, New York, 2001.
[25] B. Amaziane, A. Bourgeat, J. Koebbe, Numerical simulation and homogenization of 2-phase flow in heterogeneous porous-media, Trans. Porous Med. 6 (1991) 519–547.
[26] W. Zijl, A. Trykozko, Numerical homogenization of two-phase flow in porous media, Comput. Geosci. 6 (2002) 49–71.
[27] S.B. Pope, Turbulent Flows, Cambridge University Press, Cambridge, 2000.
[28] Y. Sun, C. Beckermann, A phase-field model of solidification with density change and convection, in preparation.
[29] I. Steinbach, F. Pezzolla, A generalized field method for multiphase transformations using interface fields, Physica D 134 (1999) 385–393.
[30] R.L. Panton, Incompressible Flow, second ed., John Wiley & Sons, New York, 1996.
[31] B. Nestler, A.A. Wheeler, L. Ratke, C. Stocker, Phase-field model for solidification of a monotectic alloy with convection, Physica D 141 (2000) 133–154.